REPORT No. 772

DETERMINATION OF GENERAL RELATIONS FOR THE BEHAVIOR OF TURBULENT BOUNDARY LAYERS

By Albert E. von Doenhoff and Neal Tetervin

SUMMARY

An analysis has been made of a considerable amount of data for turbulent boundary layers along wings and bodies of various shapes in order to determine the fundamental variables that control the development of turbulent boundary layers. It was found that the type of velocity distribution in the boundary layer could be expressed in terms of a single parameter. This parameter was chosen as the ratio of the displacement thickness to the momentum thickness of the boundary layer. The variables that control the development of the turbulent boundary layer apparently are (1) the ratio of the nondimensional pressure gradient, expressed in terms of the local dynamic pressure outside the boundary layer and boundary-layer thickness, to the local skin-friction coefficient and (2) the shape of the boundary layer. An empirical equation has been developed in terms of these variables that, when used with the momentum equation and the skin-friction relation, makes it possible to trace the development of the turbulent boundary layer to the separation point.

INTRODUCTION

A good measure of the understanding of the general problem of the flow of a real fluid about a body of arbitrary shape can be taken as the degree of approximation with which the aerodynamic characteristics of the body can be calculated on the basis of existing knowledge. The flow in regions removed from the wake and from the surface of a body obeys very closely the laws for perfect frictionless fluids at all reasonably large Reynolds numbers. This type of flow is well understood, although the detailed computations may be difficult in some cases. Departure of the flow of real fluids from that of the frictionless fluid is caused almost entirely by the failure of the idealized fluid to reproduce the actual flow conditions at the surface of the body.

Because the theory of perfect fluids gives zero drag for all bodies and gives no information concerning conditions that lead to separation of the flow from the surface, these phenomena must be almost entirely associated with the behavior of the flow at the surface or, in other words, with the boundary layer; that is, all drag, with the exception of induced drag and drag due to shock waves, all cases of flow separation such as occur at maximum lift or at high aileron deflections, and all Reynolds number effects are entirely dependent on the behavior of the boundary layer.

Because the flow of ideal fluids is well understood, the problem of calculating the actual flow resolves itself into a study of boundary layers. There are three general types of boundary layer: laminar, transitional, and turbulent. In most cases, the important laminar-boundary-layer characteristics—thickness, skin friction, and point of separation—can be estimated with sufficient accuracy from methods described in references 1 and 2. If, in unusual cases, more detailed information is required, one of the methods of calculation given in reference 3 may be used.

Experiments in low-turbulence wind tunnels and in flight have shown that extensive laminar layers may be maintained in the presence of a favorable pressure gradient. Although little is known about methods of determining the position of the transition point, transition must occur either associated with laminar separation or at some position upstream of the separation point. The position of the transition point varies widely within this region because of changes in stream turbulence, surface condition, and Reynolds number.

A considerable amount of progress has been made in determining turbulent skin friction in pipes and along flat plates with zero pressure gradient. As a result of the development of the "mixing-length" theory, notably by Prandtl and von Kármán, reliable rules that should be applicable throughout an extremely wide range of Reynolds numbers have been found for calculating the skin friction and velocity distribution in the boundary layer along flat plates and in pipes.

In order to find the effect of varying pressures on the boundary-layer characteristics, von Kármán applied the momentum theorem to the boundary layer and derived the so-called "momentum equation" that gives the rate of thickening of the boundary layer if the type of velocity distribution within the boundary layer, the external pressure distribution, and the skin friction are known. It was found in a number of cases that, if the shape of the boundary layer and the skin friction were assumed to be the same as in pipes, good agreement was obtained between the calculated and experimental boundary-layer thickness and skin friction. This procedure, however, fails to give any information concerning the changes in boundary-layer characteristics that lead to separation of the flow from the surface. In addition to the momentum equation, a relation is needed between the shape of the velocity distribution in the boundary layer, the skin friction, and the pressure distribution.

Several attempts have been made to find such a relation. From experiments in converging and diverging channels, Nikuradse, using water (reference 4), and Dönch, using air (reference 5), found that, in cases in which the boundary layer along the walls met in the center of the channel, the velocity distribution across the channel was a function of $\alpha \sqrt{R}$, where α is the angle of divergence of the channel and R is the Reynolds number based on the channel width and average velocity. Buri, whose work was discussed by Prandtl in reference 6, used the results of Nikuradse and Dönch in an attempt to calculate the general behavior of turbulent boundary layers. Buri assumed that the shape of the boundary layer was always given by the parameter of Nikuradse and Dönch. One of the weaknesses in Buri's calculations was the assumption that the shape of the velocity distribution depended only on the value of this parameter and was independent of the previous history of the boundary layer. It may be pointed out that the parameter of Nikuradse and Dönch is not essentially a shape parameter but represents a function of the pressure gradient and skin friction which is assumed to determine the shape of the velocity distribution.

Gruschwitz (reference 7), using a parameter dependent upon the type of velocity distribution in the boundary layer, found a relation between the pressure gradient and this parameter. This relation, with the momentum equation, was sufficient to determine the development of the turbulent boundary layer along a surface. Although Gruschwitz obtained good agreement with experiment for the data presented in his paper, other investigators who have tried to use the method reported poor agreement for cases in which the turbulent boundary layer separated from the surface. Peters (reference 8) conducted an investigation for the specific purpose of testing the Gruschwitz method of calculation and concluded that the Gruschwitz method cannot be used to determine the location of the separation point nor even, in many cases, to predict whether separation will occur at all.

The purpose of the present investigation is to determine the important variables that control the behavior of turbulent boundary layers and to develop general relations in terms of these variables that describe the boundary-layer motion. The fundamental variables must, of course, be expressed nondimensionally in terms of local boundary-layer quantities.

The quantities at a given station along a surface that were felt to have the most important effect on the further development of the boundary layer are the following:

(1) Shape of the boundary-layer profile
(2) Rate of change along the surface of the dynamic pressure outside the boundary layer
(3) Skin friction

Data from various published sources and from tests in the NACA two-dimensional low-turbulence tunnel made specifically for the present investigation were analyzed in terms of the foregoing variables in order to find the needed general relation for the rate of change of shape of the boundary-layer profiles.

SYMBOLS

α angle of divergence of channel; also, angle of attack
R Reynolds number
D minor axis of ellipse
u velocity within boundary layer
U_0 free-stream velocity
x distance along surface
c chord
y distance perpendicular to surface
θ momentum thickness $\left[\int_0^\infty \frac{u}{U}\left(1-\frac{u}{U}\right)dy \right]$
U velocity outside boundary layer
τ_0 skin friction per unit length
q dynamic pressure outside boundary layer
H shape-parameter
δ^* displacement thickness $\left[\int_0^\infty \left(1-\frac{u}{U}\right)dy \right]$
ρ density
$R_\theta = \dfrac{\rho \theta U}{\mu}$
μ viscosity
δ boundary-layer thickness
ν kinematic viscosity
C constant
s equivalent length of flat plate before pressure recovery begins
b width of channel
h_1 total pressure at distance θ from surface
h_0 free-stream total pressure
η shape parameter $\left[1-\left(\frac{u_\theta}{U}\right)^2 \right]$
u_θ velocity at distance θ from surface
q_0 initial value of q
C_1 constant
θ_0 initial value of θ
R_{θ_0} initial value of R_θ
$E = 2.557 \log_e 4.075 R_{\theta_0}$
$F = 2.557 \left(\dfrac{C_1}{2C} + 1 \right)$

EXPERIMENTAL DATA

The data used in the analysis were collected from the available literature and from tests performed in the NACA two-dimensional low-turbulence tunnel. The following table shows the data used in the present analysis:

Model	Reynolds number, R	Angle of attack (deg)	Reference
NACA 66,2-216	0.9×10^6 1.5 2.2 2.5 2.6	10.1 10.1 10.1 10.1 10.1	9
NACA 65(216)-222 (approx.)	.92 1.51 2.67 .92 1.51 2.64	8.1 8.1 8.1 10.1 10.1 10.1	Present report
NACA nose-opening airfoil shape 13	1.46 2.39 4.18	9.1 9.1 9.1	Present report
Channel		Run 2	7
NACA 0012	7.6	0	10
Symmetrical airfoil	3.8 (approx.)	9	8
Elliptic cylinder	.118	0	11

The paper by Gruschwitz (reference 7) contained data on a wing and on channel walls obtained from tests at Göttingen. The data from run 2 on the channel wall in the form of boundary-layer velocity profiles, pressure distribution, and curves of the momentum thickness and the shape parameter plotted against distance along the plate were used. From Peters' paper (reference 8), data were taken in the form of curves of the momentum thickness, shape parameter, and pressure coefficient against the position along the airfoil chord. These tests were made in order to check the method of calculation proposed by Gruschwitz. The [Reynolds number of the test was not given explicitly and was judged to be slightly less than 4,000,000. The results from the tests at an angle of attack of 9° were used because the data for this angle of attack were presented in a convenient form and because separation of the flow had taken place at the rear of the wing.

A few points were obtained from the boundary-layer velocity profiles and pressure distribution contained in reference 11. The data were obtained from a test of an elliptic cylinder at an angle of attack of 0° and a Reynolds number of 118,000 based on the minor axis D of the ellipse. The ratio of major to minor axis was 2.96, making the Reynolds number based on the major axis equal to 349,000.

The data on turbulent boundary layers involving separation obtained from the NACA two-dimensional low-turbulence tunnel were collected from previous tests and from tests performed specifically for the present investigation.

A few turbulent-boundary-layer profiles that were not close to separation were obtained from previously published data on the NACA 0012 airfoil (reference 10). These points were used in the analysis mainly because the boundary layer was far from separation and the use of these points helped to give a better distribution of data. The data obtained on the NACA 66,2–216 airfoil are given in reference 9. Ordinates for this section can be found by methods described in reference 12.

Tests of a thick airfoil, the NACA 65(216)–222 (approx.) were made at three Reynolds numbers at two angles of attack. The methods of obtaining the data were the same as those described in reference 9. All the tests of this airfoil involved turbulent separation. The data from these tests are presented in the form of boundary-layer velocity profiles for a number of stations along the chord (figs. 1 to 4). The pressure distributions are given in figure 5. The region of turbulent separation is indicated in the pressure distribution as the flat region at the rear of the airfoil. The chord of the airfoil was 24 inches and the airfoil was finished as described in reference 9. The ordinates can be derived by methods explained in reference 12. The finish was free from all surface imperfections that could be felt by hand but had a strip of carborundum-covered cellulose "Scotch" tape 1 inch wide on the upper surface near the leading edge.

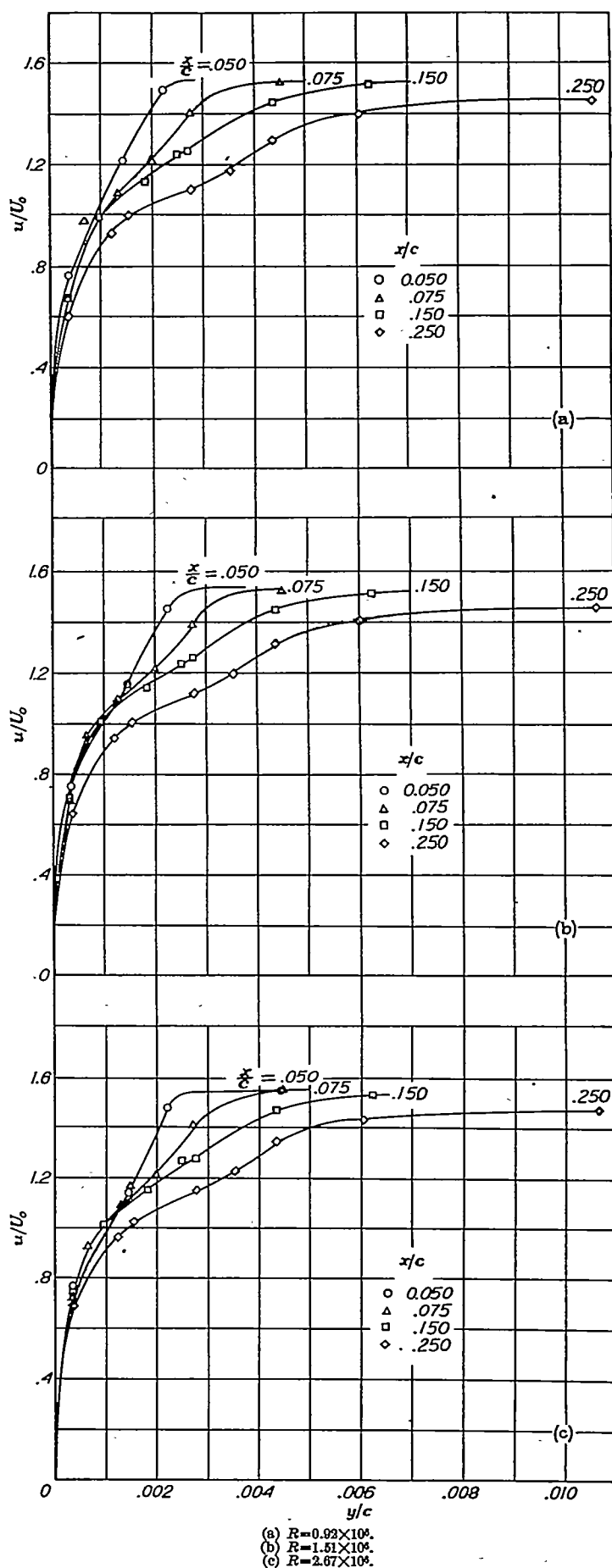FIGURE 1.—Boundary-layer velocity profiles in the region forward of the 35-percent-chord station. Airfoil section, NACA 65(216)–222 (approx.); α=8.1°.

(a) $R=0.92\times10^6$.
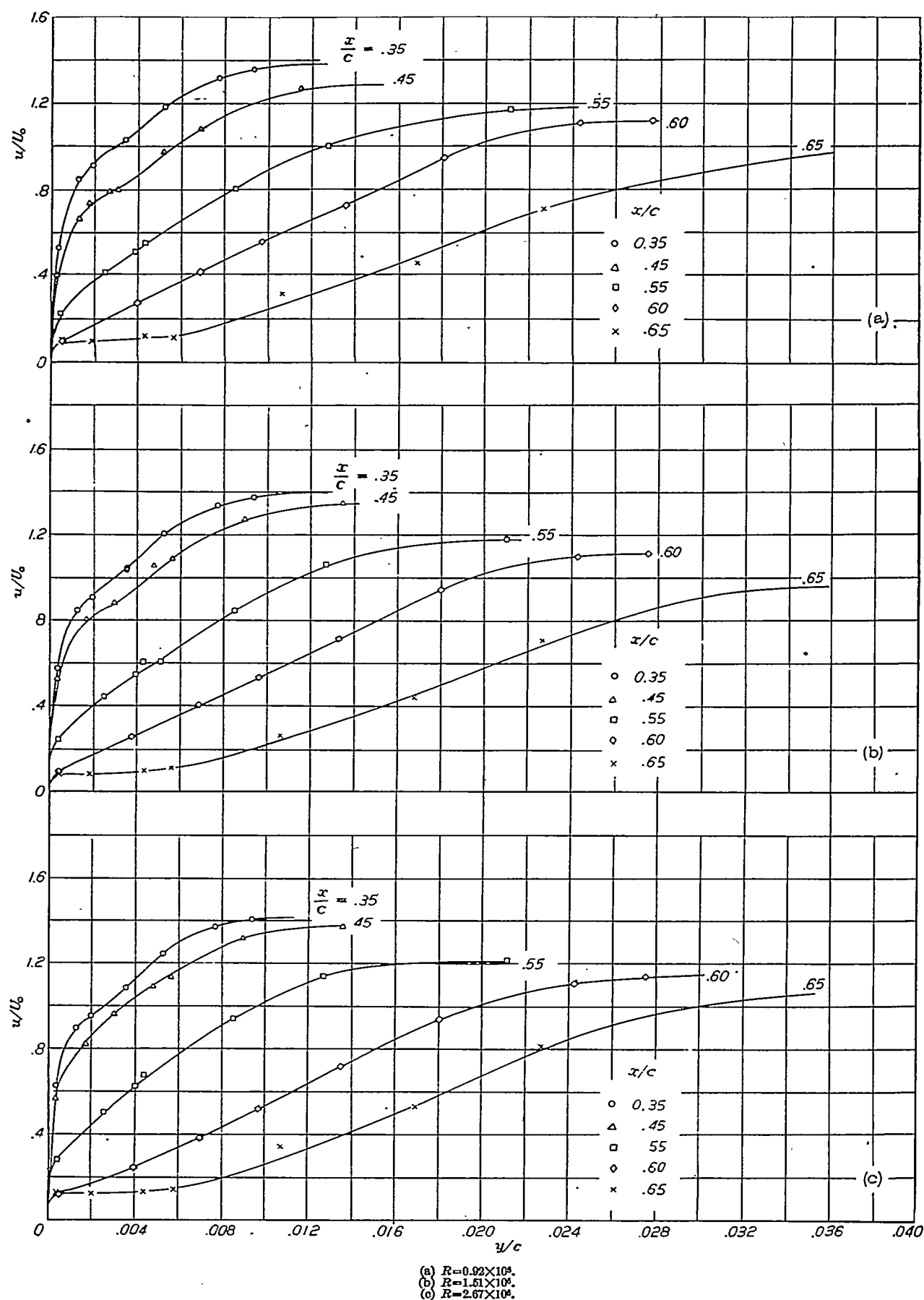(b) $R=1.51\times10^6$.
(c) $R=2.67\times10^6$.

FIGURE 2.—Boundary-layer velocity profiles in the region from the 35-percent-chord to the 65-percent-chord stations. Airfoil section, NACA 65(216)–222 (approx.); $\alpha=8.1°$.

The other model tested in the NACA two-dimensional low-turbulence tunnel for data to be used in the present analysis was the NACA nose-opening airfoil shape 13. The model had a chord of 36 inches and was finished in the same manner as the NACA 66,2–216 (reference 9). The section ordinates for the NACA nose-opening airfoil shape 13 are given in reference 13. The wing was tested at an angle of attack of 9.1° at three Reynolds numbers. The turbulent separation obtained in this test was not so marked as that obtained in the tests of the NACA 66,2–216 and NACA 65(216)–222 (approx.) airfoils, although tufts placed at the rear of the wing on the upper surface indicated separation. The data from these tests are presented in figures 6 and 7 in the form of boundary-layer velocity profiles for a number of stations along the chord. The pressure distributions are given in figure 8. The beginning of separation is indicated in the pressure distributions by the flattening of the curves at the rear of the airfoil. The small flat region in the pressure distribution at the nose of the airfoil is an indication of laminar separation. The boundary-layer velocity profiles for the region at the nose of the airfoil are shown in figure 6. The peculiar shape of the velocity distribution for some of the stations, particularly in the curves that show increasing velocity with approach toward the wall, is probably caused by spanwise flows over the airfoil. The boundary-layer thicknesses obtained in these tests were much larger than those usually obtained for airfoils of 36-inch chord.

ANALYSIS

The equation that gives the rate of change of the momentum defect in a boundary layer, originally derived by von Kármán, may be written in the following form for two-dimensional flow:

$$\frac{d\theta}{dx}+\left(\frac{H+2}{2}\right)\frac{\theta}{q}\frac{dq}{dx}=\frac{\tau_0}{2q}$$

where

θ momentum thickness $\left[\int_0^\infty \frac{u}{U}\left(1-\frac{u}{U}\right)dy\right]$

u velocity within boundary layer

U velocity outside boundary layer

y distance perpendicular to surface

τ_0 skin friction per unit length

q dynamic pressure outside boundary layer

x distance along surface

H shape parameter

The shape parameter H is defined as the ratio δ^*/θ where $\delta^*=\int_0^\infty\left(1-\frac{u}{U}\right)dy$. The difference between the actual flow of momentum in the boundary layer and that of the same quantity of fluid flowing with velocity U is $\rho U^2\theta$. From this relation, the length θ is given the name momentum thickness.

(a) $R=0.92\times10^6$.
(b) $R=1.51\times10^6$.
(c) $R=2.64\times10^6$.
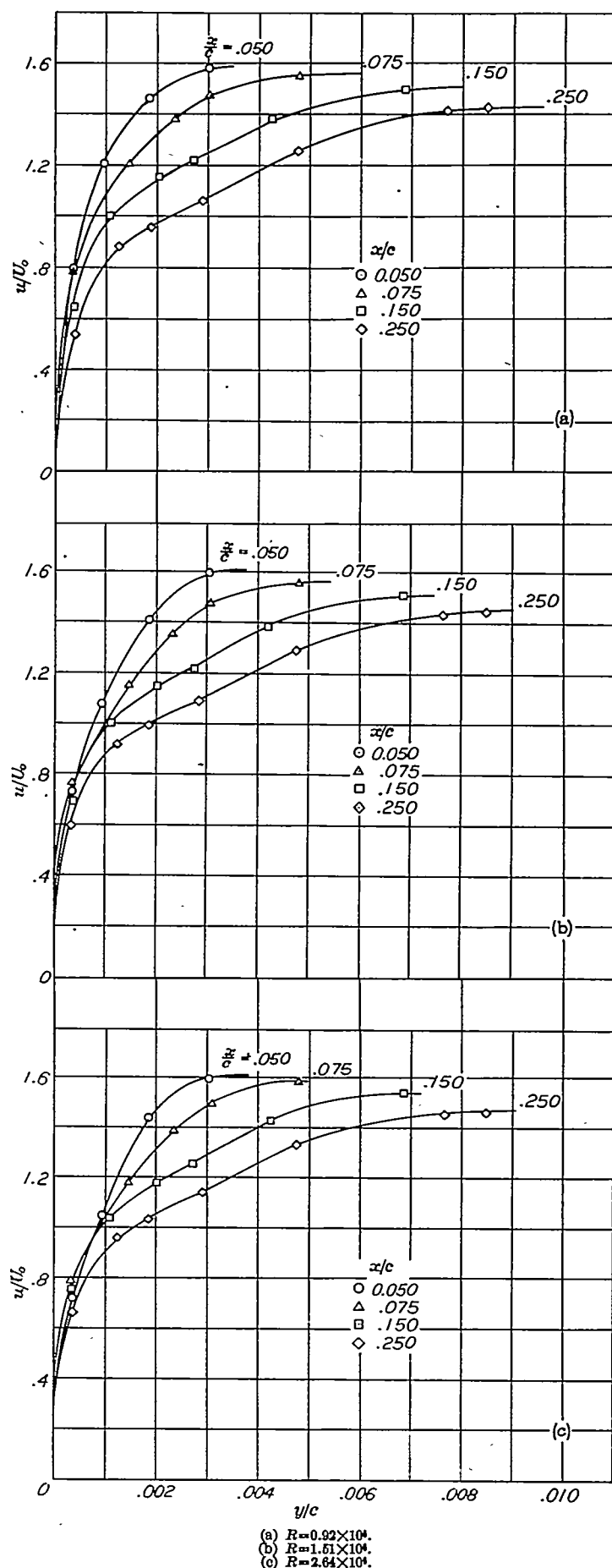
FIGURE 3.—Boundary-layer velocity profiles in the region forward of the 35-percent-chord station. Airfoil section, NACA 65(216)–222 (approx.); $\alpha=10.1°$.

(a) $R=0.92\times10^6$.
(b) $R=1.51\times10^6$.
(c) $R=2.64\times10^6$.

FIGURE 4.—Boundary-layer velocity profiles in the region from the 35-percent-chord to the 65-percent-chord stations. Airfoil section, NACA 65(216)-222 (approx.); $\alpha=10.1°$.

(a) $\alpha = 8.1°$.
(b) $\alpha = 10.1°$.
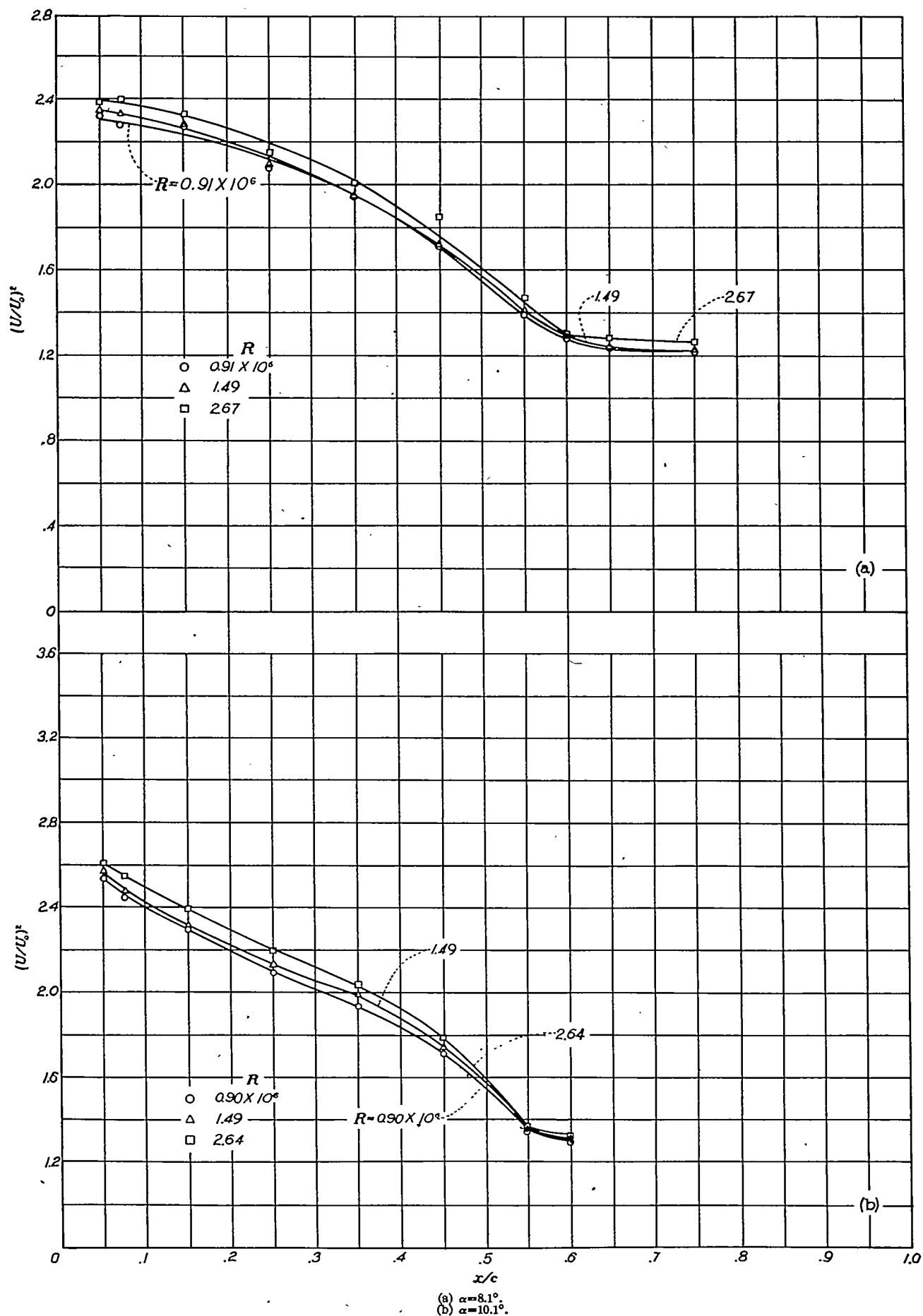
FIGURE 5.—Upper-surface pressure distributions for several Reynolds numbers.   Airfoil section, NACA 65(216)-222 (approx.).
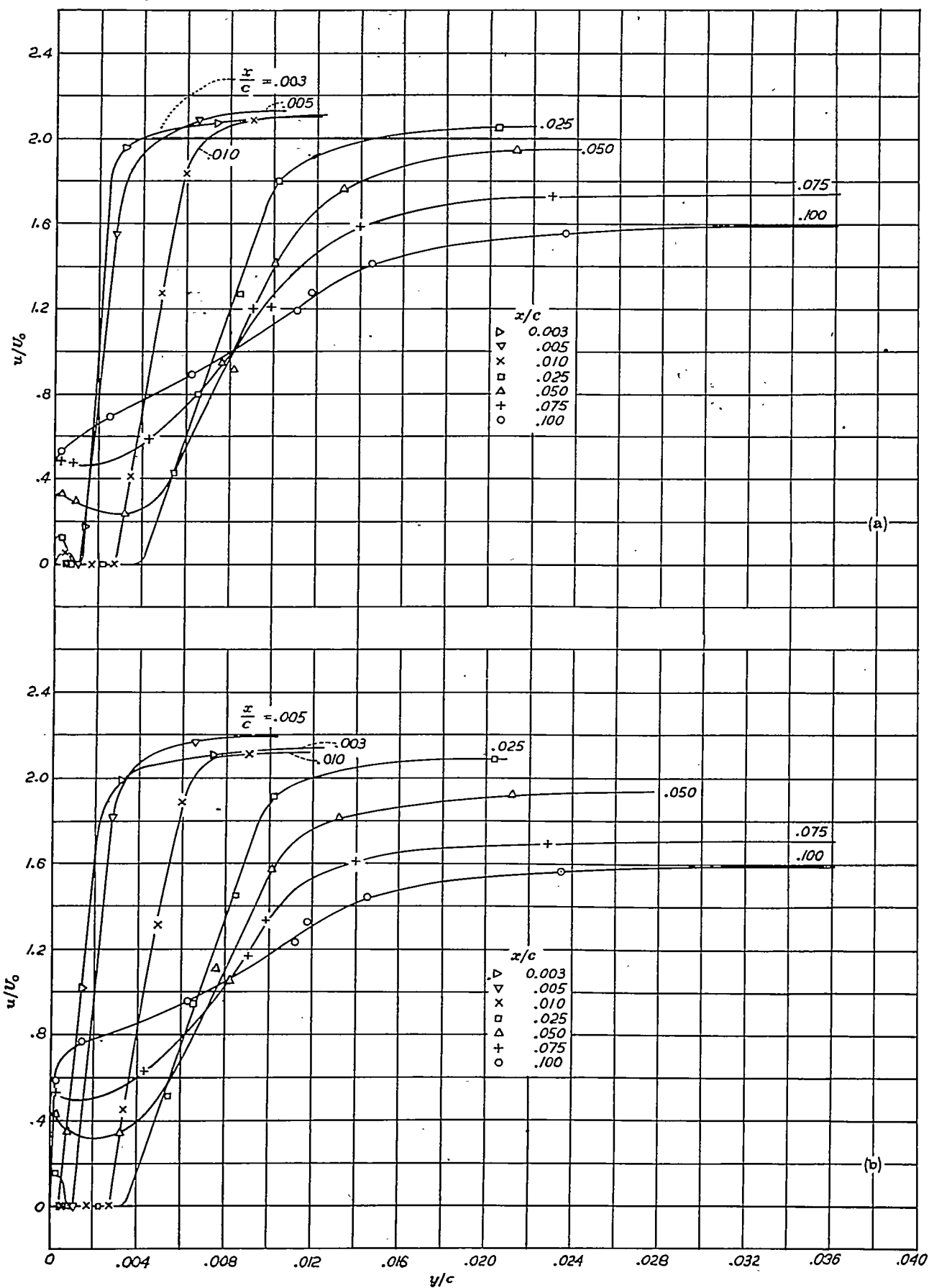
(a) $R=1.46\times10^6$.
(b) $R=2.39\times10^6$.

FIGURE 6.—Boundary-layer velocity profiles in the region forward of the 10-percent-chord station.   Nose-opening airfoil shape 13; $\alpha=9.1°$.

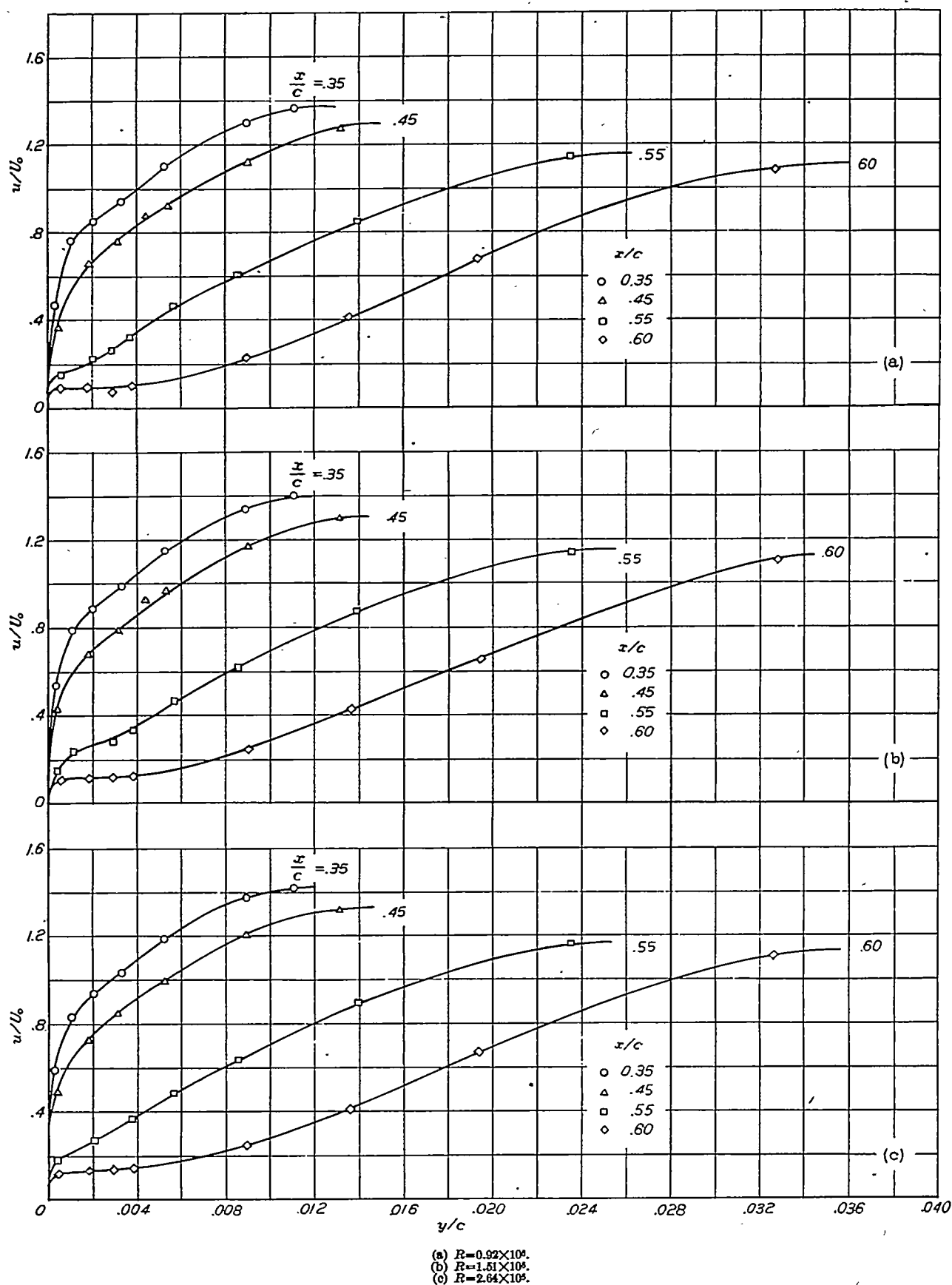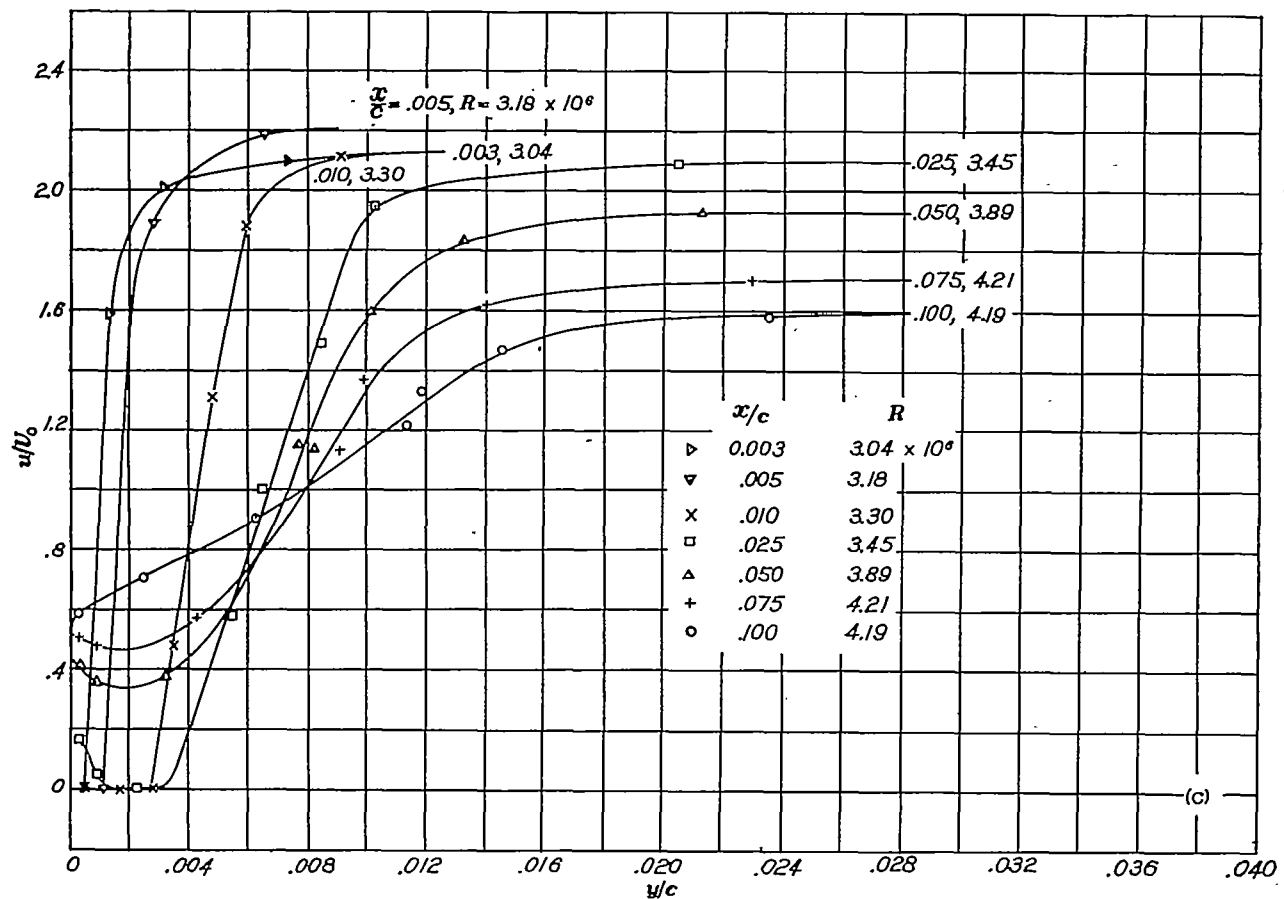(c) At several Reynolds numbers.

FIGURE 6.—Concluded.
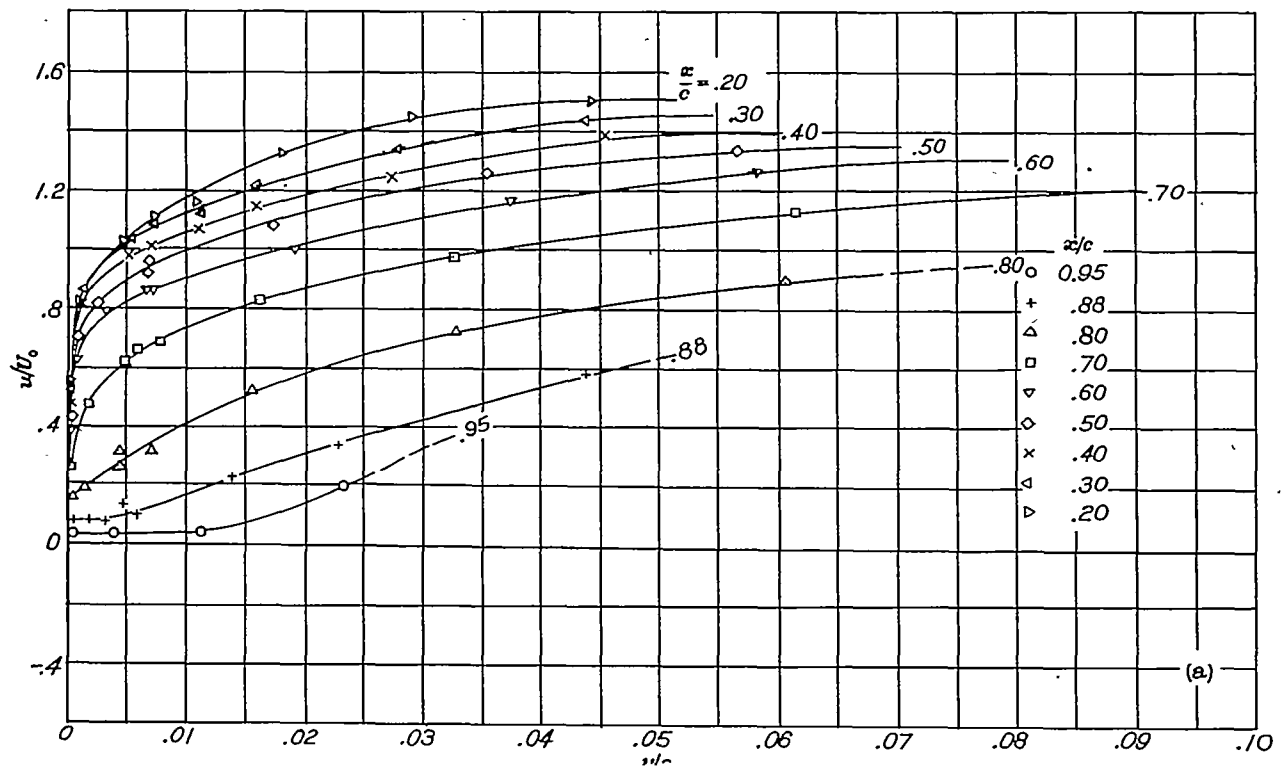
(a) $R = 1.46 \times 10^6$.

FIGURE 7.—Boundary-layer velocity profiles in the region from the 20-percent-chord to the 95-percent-chord stations.   Nose-opening airfoil shape 13; $\alpha = 9.1°$.
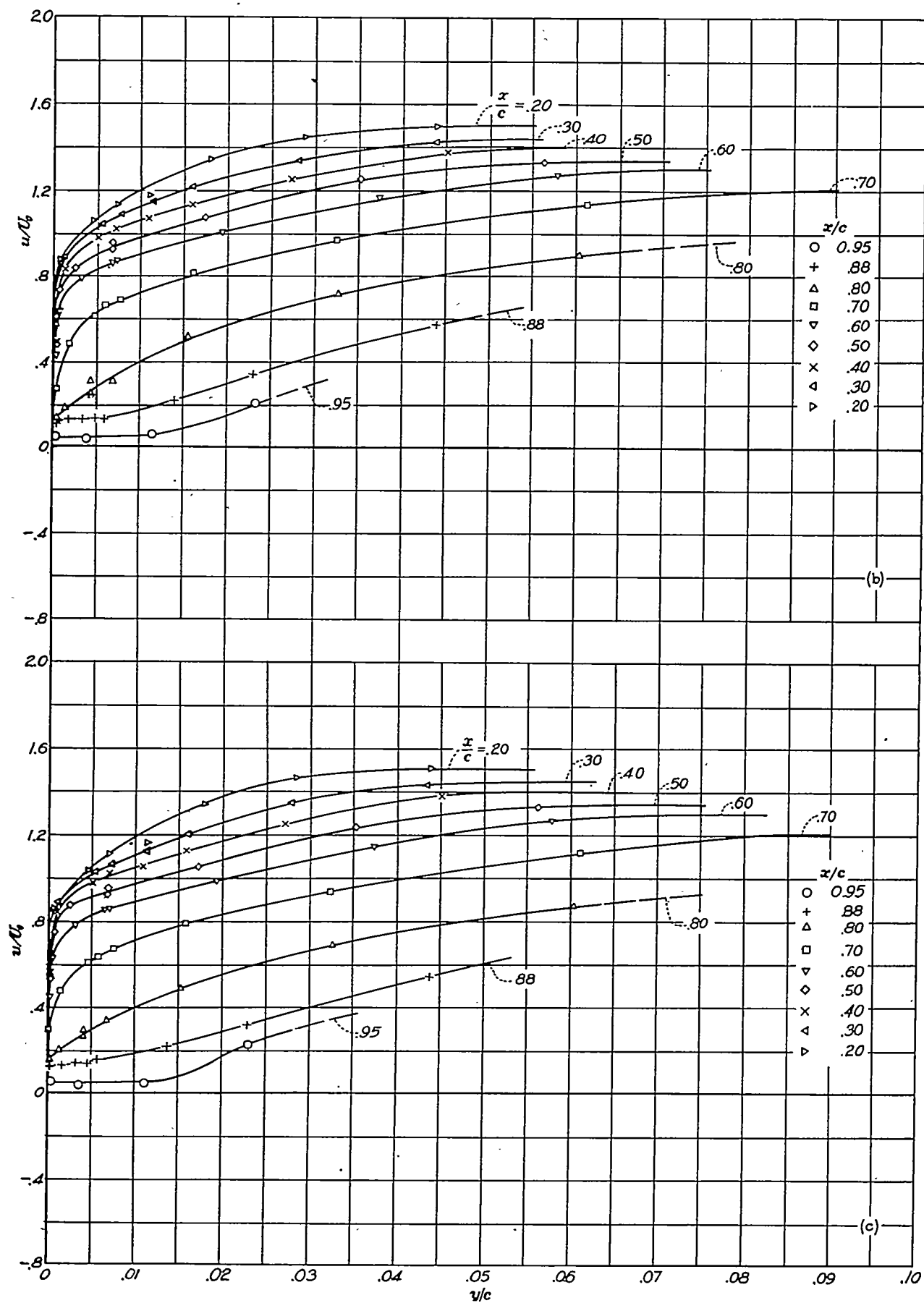
(b) $R=2.39\times10^{6}$.
(c) $R=4.18\times10^{6}$.

FIGURE 7.—Concluded.

$$\left(\frac{u}{U_0}\right)^2$$
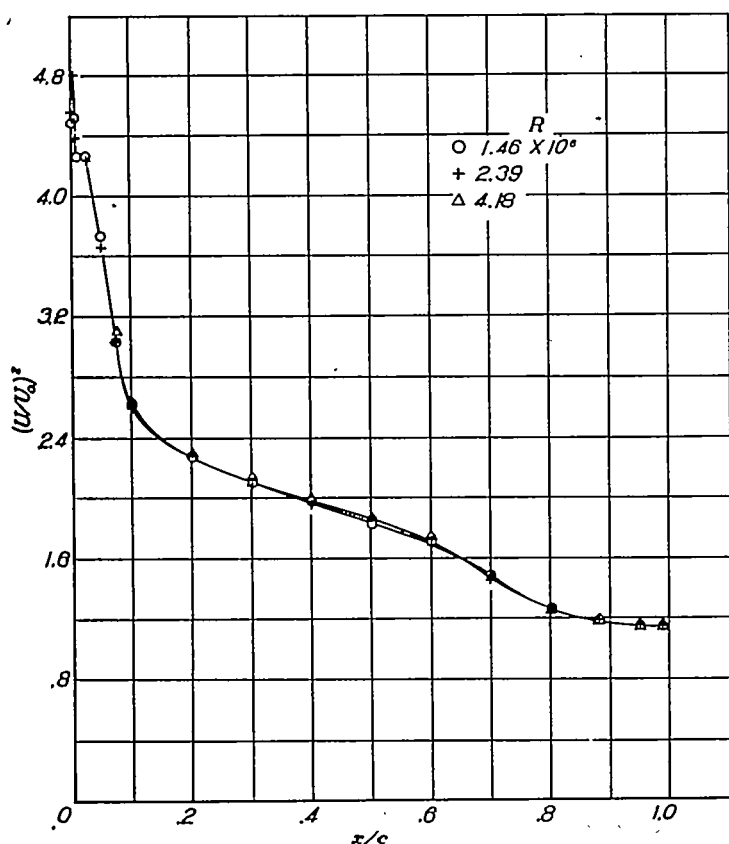
R	
O	1.46 × 10⁶
+	2.39
△	4.18

FIGURE 8.—Upper-surface pressure distributions for several Reynolds numbers. Nose-opening airfoil shape 13; α=9.1°.

The length δ^*, called the displacement thickness, is the amount by which the streamlines just outside the boundary layer are displaced because of the reduction of velocity within the boundary layer. Because θ depends on the second power of the velocity distribution, whereas δ^* depends on only the first power, the ratio δ^*/θ depends on the manner in which u/U varies with y— that is, upon the shape of the boundary-layer profile.

The momentum equation in the form just given contains only local boundary-layer quantities. The local skin-friction coefficient is τ_0/q. The nondimensional pressure gradient is $\frac{\theta}{q}\frac{dq}{dx}$, where θ is the unit of length and q is the unit of dynamic pressure.

Although it has been shown that the shape of the boundary-layer profile determines H, the converse cannot be proved from mathematical considerations alone. If H does actually determine the shape of the boundary-layer profile, then all points of u/U plotted against H at a constant value of y/θ should fall on a single curve. A collection of such curves for various values of y/θ is shown in figure 9. The data presented in figure 9 represent the collection of all the boundary-layer profiles that enter into the analysis. Figure 9 shows that u/U is a function of H alone for a given value of y/θ. This conclusion is important because it means that turbulent-boundary-layer profiles form a single-parameter family of curves. The complete velocity distribution in the boundary layer is known when θ and H have been determined. Figure 10, which is a cross plot of figure 9, gives turbulent-boundary-layer velocity profiles corresponding to various

values of H. As the separation point is approached, the value of H increases. Because the turbulent separation point usually is not very well defined, it is not possible to give an exact value of H corresponding to separation. The value of H usually varies so rapidly near the separation point, however, that it is not necessary to fix accurately the value of H corresponding to separation. Separation has not been observed for a value of H less than 1.8 and appears definitely to have occurred for a value of H of 2.6. Gruschwitz's criterion for imminent separation is equivalent to a value of H of 1.85.

The fact that the type of velocity distribution in the boundary layer can be given in terms of a single parameter greatly simplifies the study of turbulent boundary layers. It is now necessary to determine only the manner in which this parameter varies along the surface as a function of the external forces acting on the boundary layer.

The external forces acting on the boundary layer at any point are the pressure gradient, expressed nondimensionally as $\frac{\theta}{q}\frac{dq}{dx}$, and the skin friction, expressed nondimensionally as τ_0/q. The assumption is made that the rate of change of H rather than H itself is related to the local forces. This assumption is desirable in order that the boundary-layer conditions downstream from a point shall be definitely connected with the conditions upstream of the point; that is, a sudden change in the pressure gradient should not produce a discontinuity in the type of velocity distribution in the boundary layer. Prandtl (reference 6) has pointed out this difficulty both in the Pohlhausen theory for laminar boundary layers and in Buri's method for calculating turbulent boundary layers. Expressed in nondimensional form, the rate of change of H is given as $\theta\frac{dH}{dx}$.

In the early stage of the analysis, the experimental data were plotted in the form of $\theta\frac{dH}{dx}$ against $\frac{\theta}{q}\frac{dq}{dx}$. Fair correlation was obtained for a limited amount of data. As the analysis was extended to include more data, systematic variations with Reynolds number were noticed. When $\theta\frac{dH}{dx}$ was plotted against $\frac{\theta}{q}\frac{dq}{dx}\frac{2q}{\tau_0}$, the consistent variation with Reynolds number was eliminated. The skin friction was tentatively assumed to be given by the Squire and Young formula (reference 14)

$$\frac{2q}{\tau_0}=[5.890\ \log_{10}\ (4.075R_\theta)]^2$$

where

$$R_\theta=\frac{\rho\theta U}{\mu}$$

This formula was chosen because of the good agreement obtained between the experimental drag coefficients for airfoils and those calculated by the Squire and Young method. It was felt that the local skin-friction coefficients thus determined were probably more accurate in most cases than those determined directly from the boundary-layer surveys.
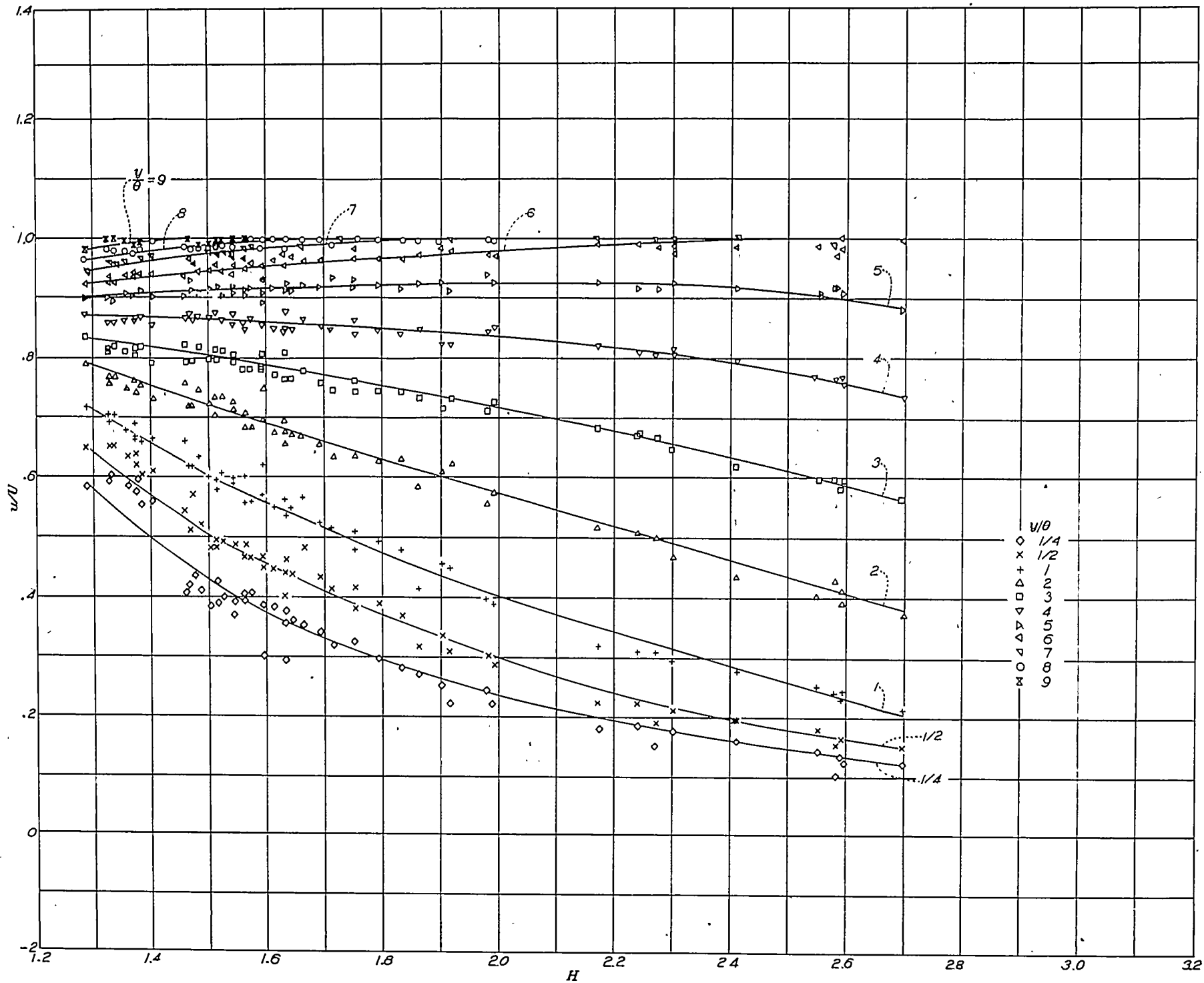
FIGURE 9.—Variation of u/U with H for various values of y/θ.
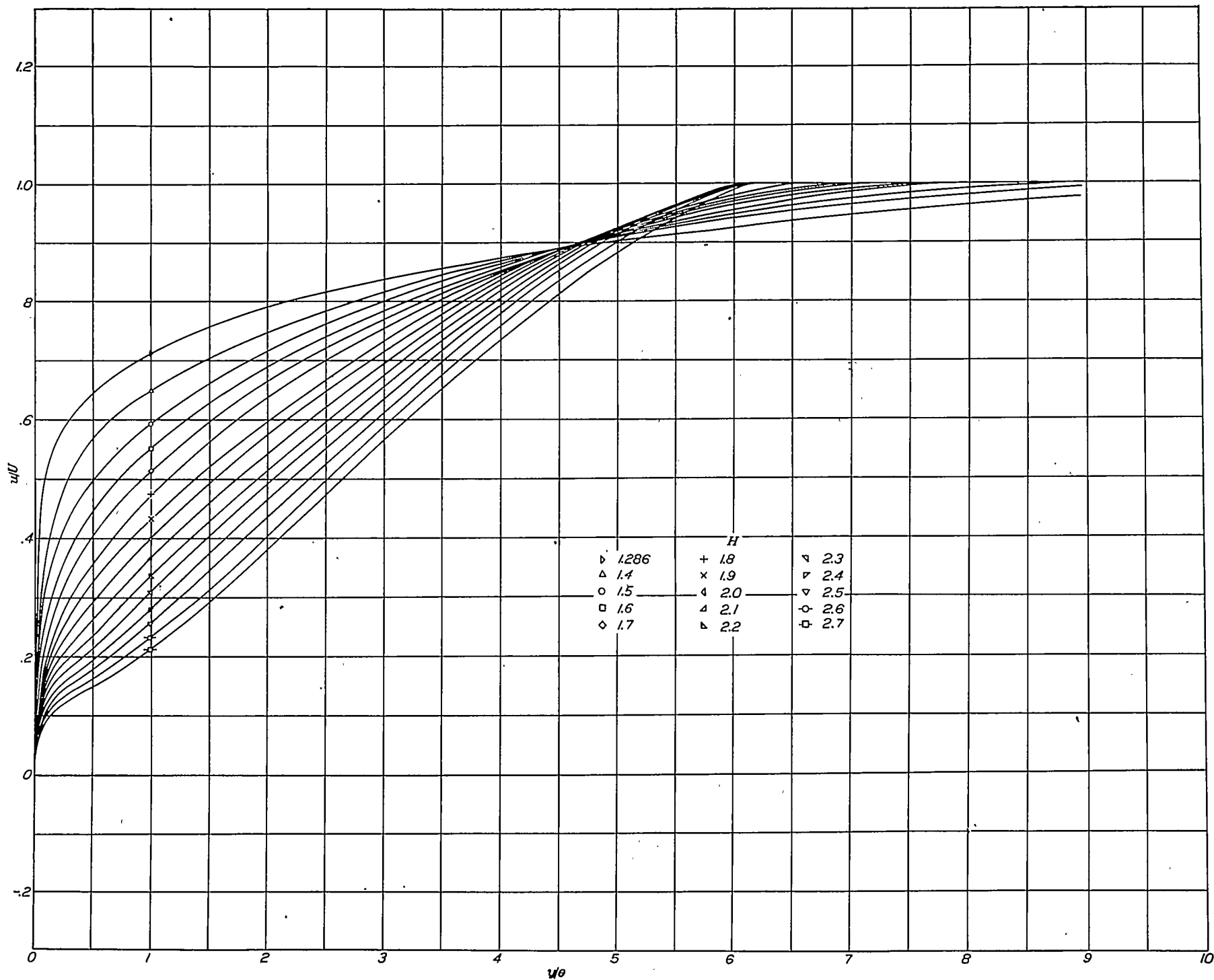
FIGURE 10.—Velocity profiles for turbulent boundary layers corresponding to various values of H.

The quantity $\frac{\theta}{q}\frac{dq}{dx}\frac{2q}{\tau_0}$, or a quantity differing only by a constant factor, has frequently been used as a parameter for boundary-layer phenomena. · For example, the Pohlhausen parameter for laminar boundary layers $\frac{\delta^2}{\nu}\frac{dU}{dx}$, where δ is the boundary-layer thickness and ν the kinematic viscosity, can be shown to be equivalent to $\frac{\theta}{q}\frac{dq}{dx}\frac{2q}{\tau_0}$. For a laminar boundary layer, $\tau_0 = \mu\left(\frac{du}{dy}\right)_0$ and $\left(\frac{du}{dy}\right)_0$ is proportional to U/δ. It thus follows that μ/δ is proportional to τ_0/U. Substituting $\frac{\tau_0}{\rho U}$ for $\frac{\mu}{\rho\delta}$ in the Pohlhausen parameter and replacing $\frac{dU}{dx}$ by its equivalent $\frac{U}{2q}\frac{dq}{dx}$ gives a quantity proportional to the Pohlhausen parameter $C\frac{\delta}{q}\frac{dq}{dx}\frac{q}{\tau_0}$, which in turn is equal to some constant times $\frac{\theta}{q}\frac{dq}{dx}\frac{2q}{\tau_0}$. By a similar process of reasoning, the parameter $\frac{s}{U}\frac{dU}{dx}$, where s is the equivalent length of the flat plate before pressure recovery is begun, which determines the amount of pressure that can be recovered in a laminar layer with a straight-line velocity gradient as given in reference 1, can be shown to be proportional to $\frac{\theta}{q}\frac{dq}{dx}\frac{2q}{\tau_0}$. Nikuradse (reference 4) found that his results for turbulent flow, which give the velocity distribution across diverging or converging channels, agreed with similar measurements made by Dönch (reference 5) when $\alpha\sqrt{R}$ had the same value. For a given type of velocity distribution across the channel, $\frac{b}{q}\frac{dq}{dx}$ at the center is proportional to the angle of divergence, where b is the width of the channel. Within the range of Reynolds numbers covered by the investigations of Nikuradse and Dönch, the skin-friction coefficient τ_0/q at the wall was inversely proportional to $\sqrt{R}$. For a given type of velocity distribution, $\alpha\sqrt{R}$ is therefore proportional to $\frac{\theta}{q}\frac{dq}{dx}\frac{2q}{\tau_0}$. It may be pointed out that, although in Buri's theory of turbulent boundary layers and Pohlhausen's theory of laminar boundary layers $\frac{\theta}{q}\frac{dq}{dx}\frac{2q}{\tau_0}$ was assumed to determine the type of velocity distribution in the boundary layer, in the present analysis it is assumed that $\frac{\theta}{q}\frac{dq}{dx}\frac{2q}{\tau_0}$ affects only the rate of change of the type of velocity distribution.

It seemed highly probable that the rate of change of H should depend not only on the ratio of the pressure gradient to the skin friction but also on the value of H itself. Plots were therefore made of $\theta\frac{dH}{dx}$ against $\frac{\theta}{q}\frac{dq}{dx}\frac{2q}{\tau_0}$ at 0.1 intervals of H for all the data entering into the present analysis. These plots are given in figure 11. Although the points show considerable scatter, definite trends for the variation of $\theta\frac{dH}{dx}$ with both $\frac{\theta}{q}\frac{dq}{dx}\frac{2q}{\tau_0}$ and H are observable. It may be pointed out, however, that both $\frac{dH}{dx}$ and $\frac{dq}{dx}$ were the slopes of experimentally determined curves. Large scatter of the data therefore is to be expected. The large scatter of the points in figure 11, consequently, does not necessarily indicate any serious inadequacies in the present analysis. From a study of the available data, it was found that the variation of $\theta\frac{dH}{dx}$ with $\frac{\theta}{q}\frac{dq}{dx}\frac{2q}{\tau_0}$ and H could be fairly well represented by the equation

$$\theta\frac{dH}{dx}=e^{4.680(H-2.975)}\left[-\frac{\theta}{q}\frac{dq}{dx}\frac{2q}{\tau_0}-2.035(H-1.286)\right]$$

The exponential form of the factor multiplying the second member of this equation was chosen because the data for high values of H, although not very complete, nevertheless indicated that $\frac{dH}{dx}$ was large. It may be noted that 1.286 is the value of H for the $\frac{1}{7}$-power distribution of velocity in the boundary layer. It is seen from the foregoing equation that no change in H is indicated for the case in which $\frac{dq}{dx}=0$ and H has the value 1.286. The degree to which the equation for $\theta\frac{dH}{dx}$ approximates the experimental data from which it was derived may be seen in figure 11. Each of the straight lines in figure 11 was obtained from the equation for $\theta\frac{dH}{dx}$ by giving H successive values of 1.35, 1.45, 1.55, and 1.65. The slope of these lines is given by the factor $e^{4.680(H-2.975)}$, and the intercept for $\theta\frac{dH}{dx}=0$ is given by the term $-2.035\,(H-1.286)$.

COMPARISON OF PRESENT ANALYSIS WITH GRUSCHWITZ ANALYSIS

In reference 7, Gruschwitz analyzes the behavior of turbulent boundary layers in the following manner:

$$\frac{\theta}{q}\frac{dh_1}{dx}=F(\eta, R_\theta)$$

where

η shape parameter $\left[1-\left(\frac{u_\theta}{U}\right)^2\right]$, in the same sense as H

u_θ velocity at $y=\theta$

and

h_1 total pressure at distance θ from surface (g_1 in reference 7)
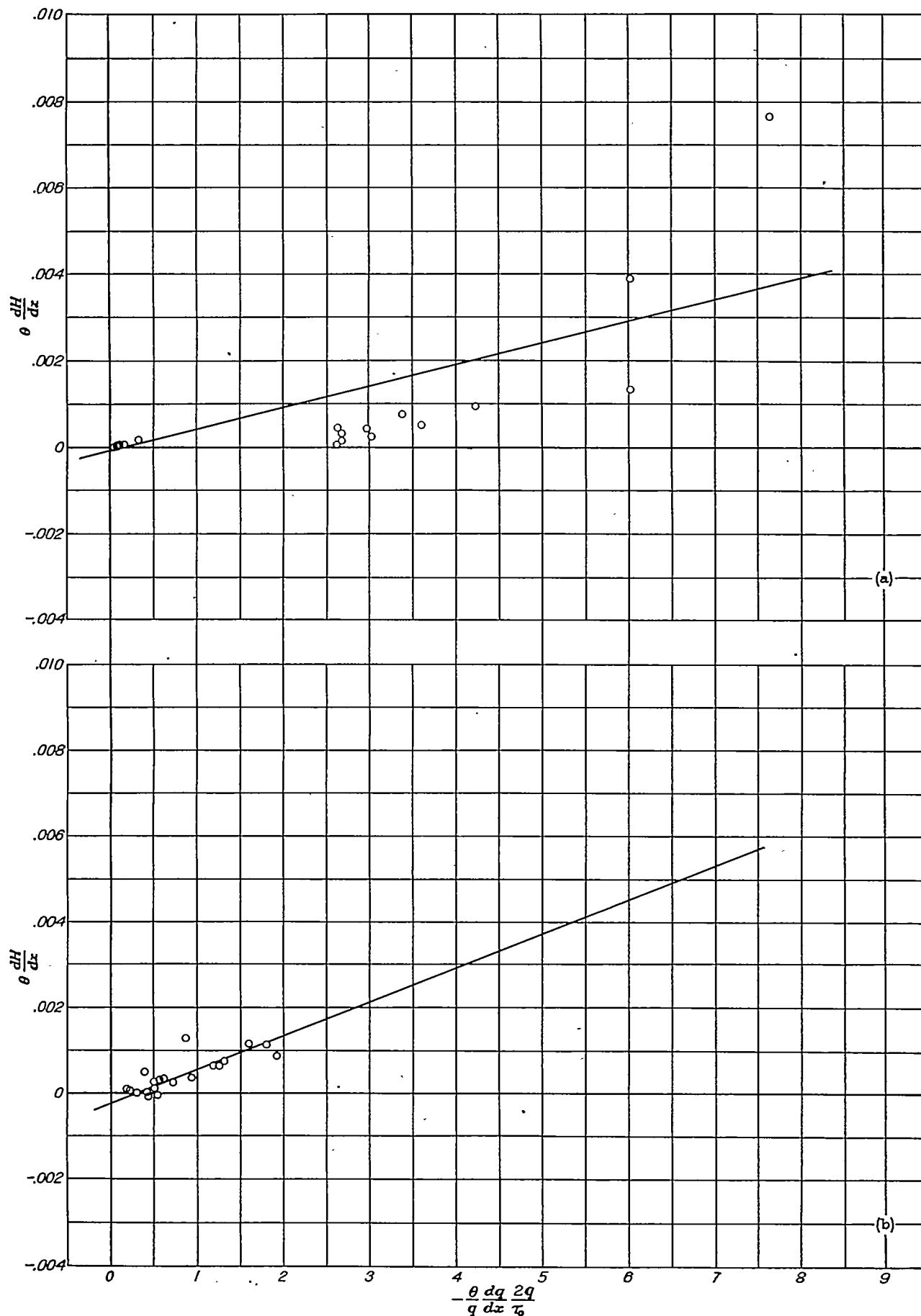
(a) Values of H from 1.3 to 1.4.
(b) Values of H from 1.4 to 1.5.

FIGURE 11.—Rate of change of H as a function of $\frac{\theta}{q}\frac{dq}{dx}\frac{2q}{\tau_0}$ and H.
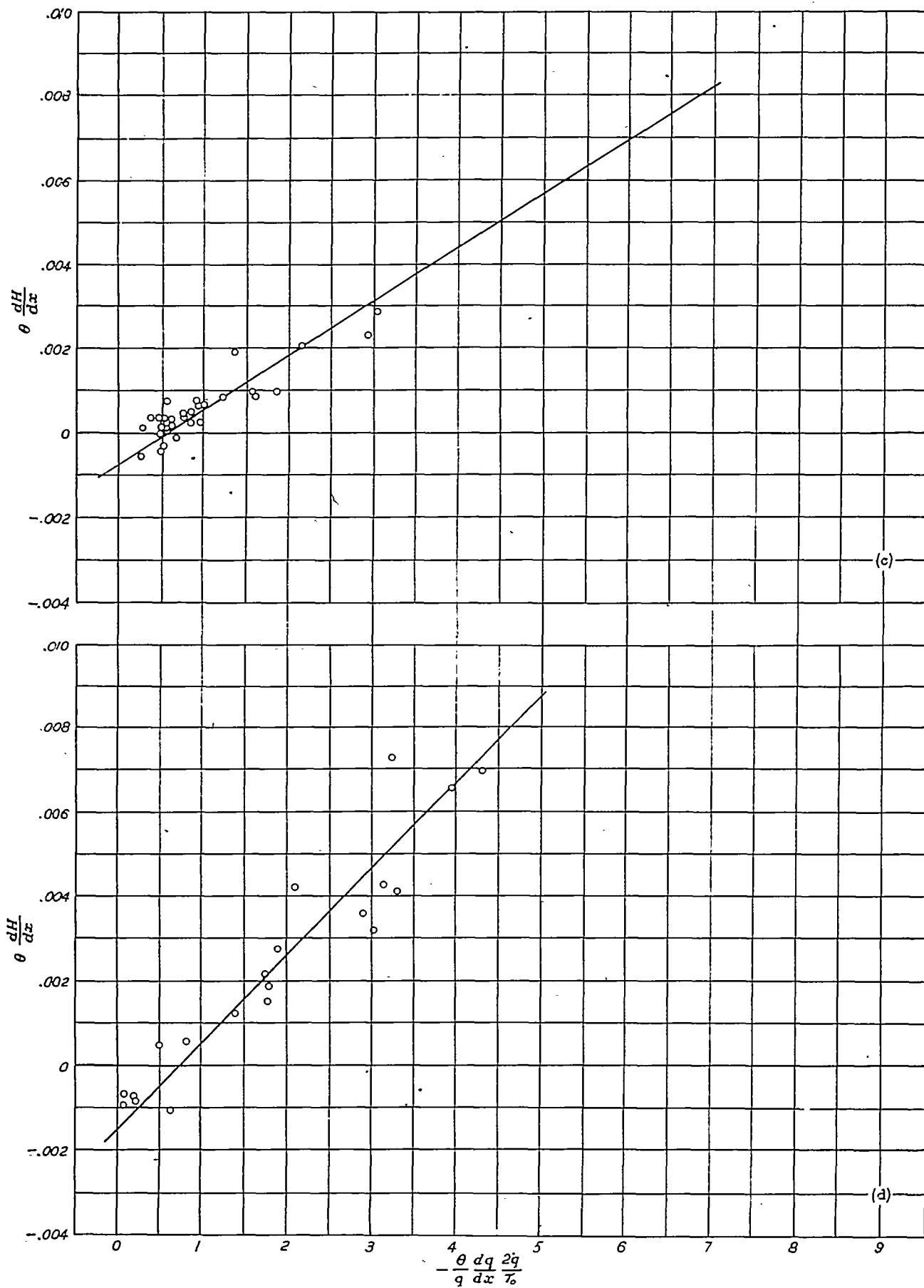
(c) Values of H from 1.5 to 1.6.
(d) Values of H from 1.6 to 1.7.

FIGURE 11.—Concluded.

In writing this relation, it is implicitly assumed that $\theta \frac{dh_1}{dx}$ is independent of $\frac{\theta}{q}\frac{dq}{dx}$. Because of this assumption, the Gruschwitz analysis is subject to the same criticism as are the Buri and Pohlhausen methods for making boundary-layer calculations. Now

$$\eta q = h_0 - h_1$$

where h_0 (g_0 in reference 7) is the free-stream total pressure; hence,

$$\frac{\theta}{q}\frac{dh_1}{dx} = -\theta \frac{d\eta}{dx} - \frac{\theta}{q}\frac{dq}{dx}\eta$$

and therefore

$$\theta \frac{d\eta}{dx} = -\frac{\theta}{q}\frac{dq}{dx}\eta - F(\eta, R_\theta)$$

Except for the factor $2q/\tau_0$, this relation is similar in form to the relation found from the present investigation; namely,

$$\theta \frac{dH}{dx} = F\left(\frac{\theta}{q}\frac{dq}{dx}\frac{2q}{\tau_0}, H\right)$$

The Gruschwitz relation, however, is very restricted in the form of the dependence of $\theta \frac{d\eta}{dx}$ on $\frac{\theta}{q}\frac{dq}{dx}$ in comparison with the type of relation used in the present investigation. Furthermore, no variation of $\theta \frac{d\eta}{dx}$ with R_θ is indicated in the final equations given by Gruschwitz.

In the Gruschwitz analysis, the arbitrary function which was to be determined experimentally contained only one variable η; whereas, in the present analysis, the arbitrary function contains two variables, $\frac{\theta}{q}\frac{dq}{dx}\frac{2q}{\tau_0}$ and H. Apart from the neglect of R_θ, one reason for the failure of the Gruschwitz analysis is that a correlation of all turbulent-boundary-layer data in terms of a function containing only one independent variable was not possible.

METHOD OF CALCULATION

For calculating the characteristics of turbulent boundary layers, the following information is required: The initial values of θ and H, the pressure distribution over the body, and the Reynolds number. The equations that are used in making a computation are

$$\frac{d\theta}{dx} + \frac{H+2}{2}\frac{\theta}{q}\frac{dq}{dx} = \frac{\tau_0}{2q}$$

$$\theta\frac{dH}{dx} = e^{4.680(H-2.975)}\left[-\frac{\theta}{q}\frac{dq}{dx}\frac{2q}{\tau_0} - 2.035\,(H-1.286)\right]$$

$$\frac{2q}{\tau_0} = [5.890\log_{10}(4.075\,R_\theta)]^2$$

In order to reduce the work of computation, $\tau_0/2q$ was plotted against R_θ in figure 12 and the factor $e^{4.680(H-2.975)}$ in the equation for $\frac{dH}{dx}$ was plotted against H in figure 13.

The momentum equation and the equation for $\frac{dH}{dx}$ are simultaneous first-order differential equations that can be

solved by a step-by-step calculation. It is usually necessary to use such a method although, for some particular cases, the equations may be integrated directly. The method of calculation is as follows: The values of the variables entering into the computation at the initial station are substituted in the momentum equation and the equation for $\frac{dH}{dx}$. Values for $\frac{d\theta}{dx}$ and $\frac{dH}{dx}$ are thus obtained at the initial station. An increment of the length along the surface of the body x is then chosen and multiplied by $\frac{d\theta}{dx}$ and $\frac{dH}{dx}$ to give $\Delta\theta$ and ΔH, respectively. These increments of θ and H are added to the initial values and result in values of θ and H for the new value of x. The process is repeated until the desired result has been attained. Separation may be considered to have occurred when H rises to about 2.6.

The choice of the increment of x is a matter for the judgment of the individual investigator. As a general rule, the increments of x should be made small when $\frac{d\theta}{dx}$ or $\frac{dH}{dx}$ changes rapidly from one value of x to the next. In order to decrease the length of the calculation, the increments of x must be chosen as large as is compatible with the accuracy desired. For the computations that were made in order to check the method of calculation, the increment of x for one step was so chosen that $\Delta\frac{dH}{dx}\Delta x < 0.0025$, where $\Delta\frac{dH}{dx}$ is the change in $\frac{dH}{dx}$ between two successive values of x and Δx is the increment of x. This criterion furnishes a measure of the maximum error that can be expected in ΔH for one step of the computation. When the flow approaches separation, H usually increases very rapidly and, in such cases, the foregoing criterion may be disregarded without appreciable error in the position of the separation point. By disregarding the criterion when the flow is close to separation, the length of the computation may be reduced.

A sample calculation for the NACA 65(216)–222 (approx.) airfoil section at $\alpha=10.1°$ and at $R=2.64\times10^6$ is given in table I.

If the question of separation is not involved and if the variation of H along the surface is not of interest, reasonably accurate values of θ may be obtained by assuming a constant value of H and merely using the momentum equation together with the skin-friction relation to determine θ. This procedure is substantially the same as that of reference 14 where a constant value of H of 1.4 was chosen for calculating the profile drag of airfoil sections.

TESTS OF METHOD OF CALCULATION

In order to obtain a general check of the method of calculation and to determine whether the scatter of the points in figure 11 was primarily due to the difficulty in obtaining the slopes of experimental curves or to serious inadequacies in the analysis, computations were carried through for eight cases. For all these computations, the initial values of H and θ were obtained from experimental data.
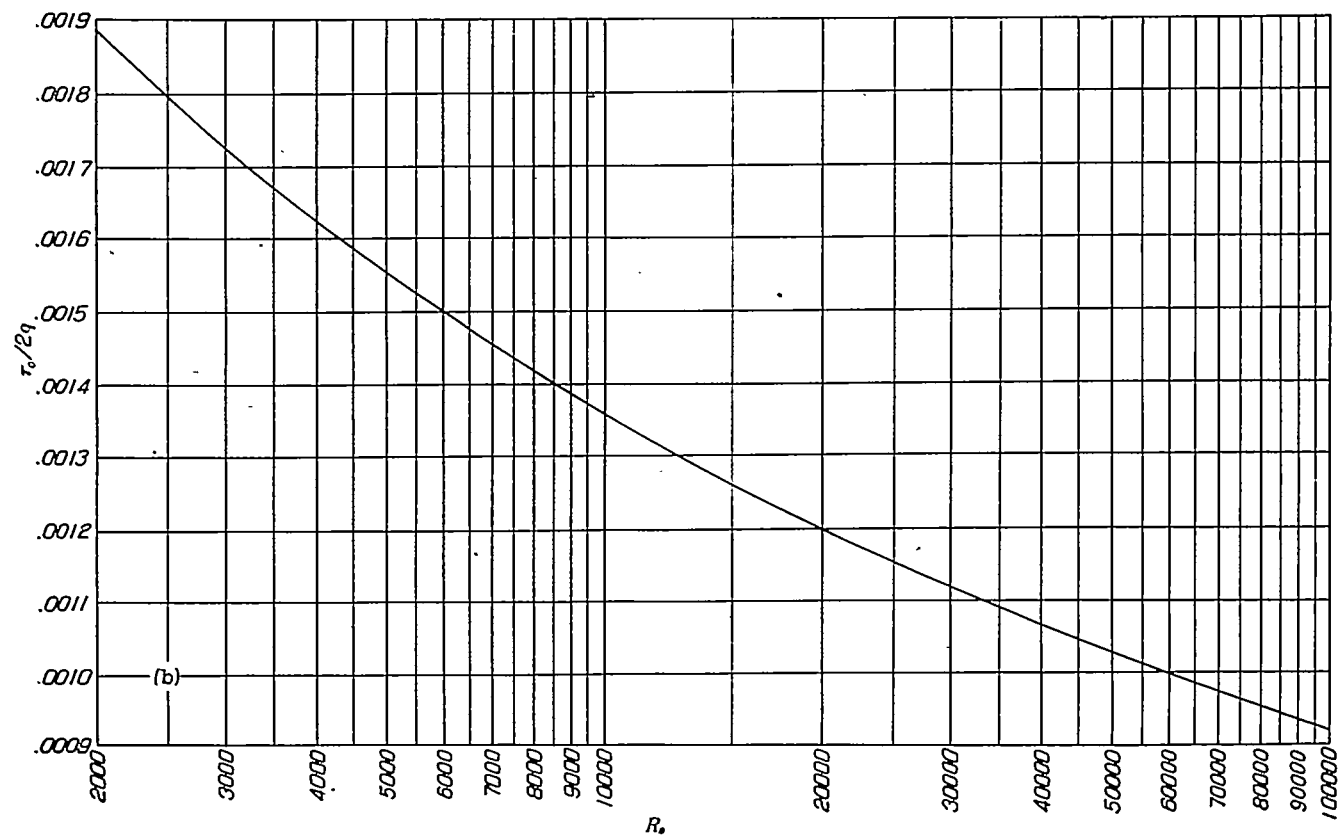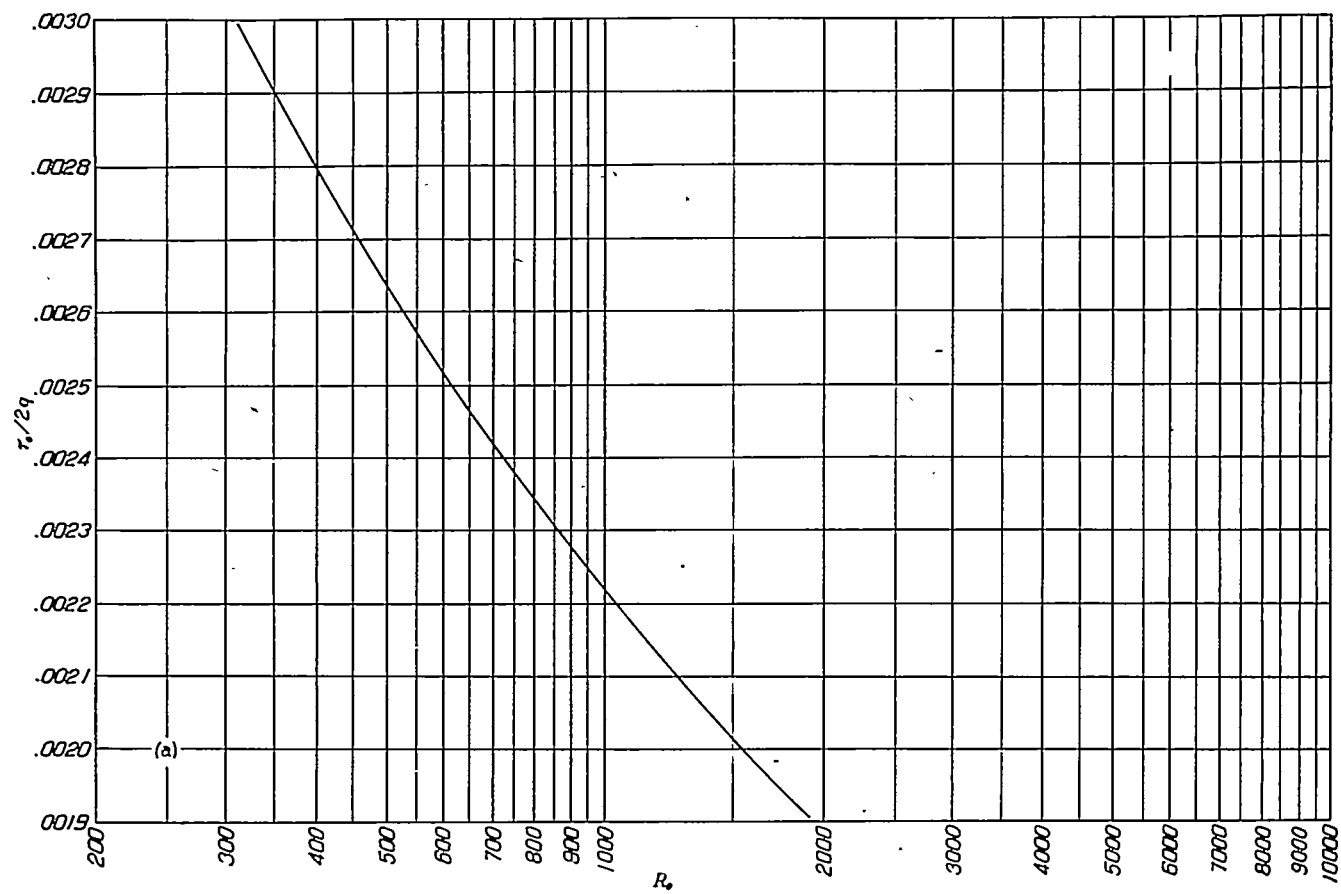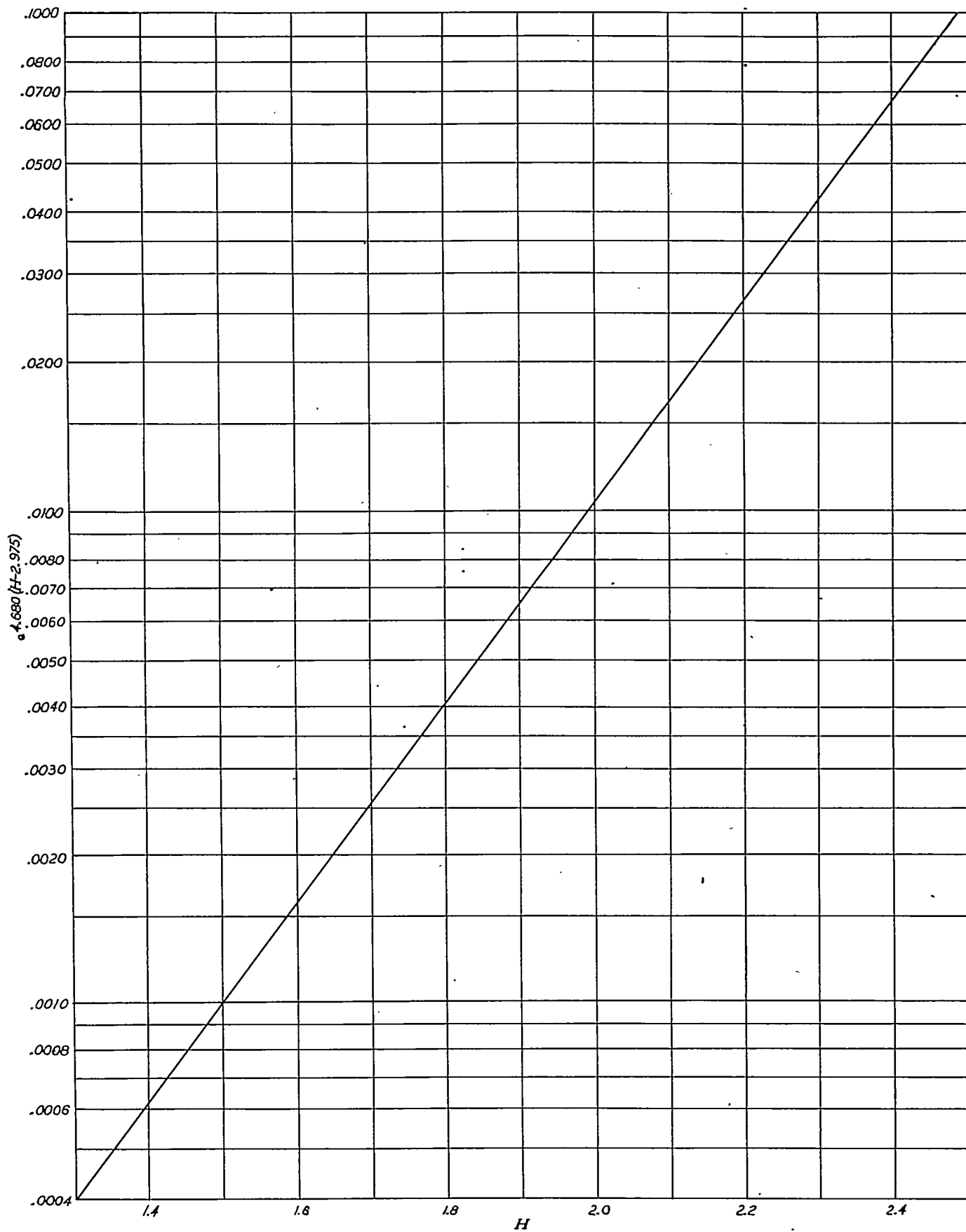
FIGURE 12.—Variation of $\tau_0/2q$ with R_θ (reference 14

FIGURE 1'.—Variation of $e^{4.680(H-2.975)}$ with H.

(a) Shape parameter H.
(b) Momentum thickness θ/c.
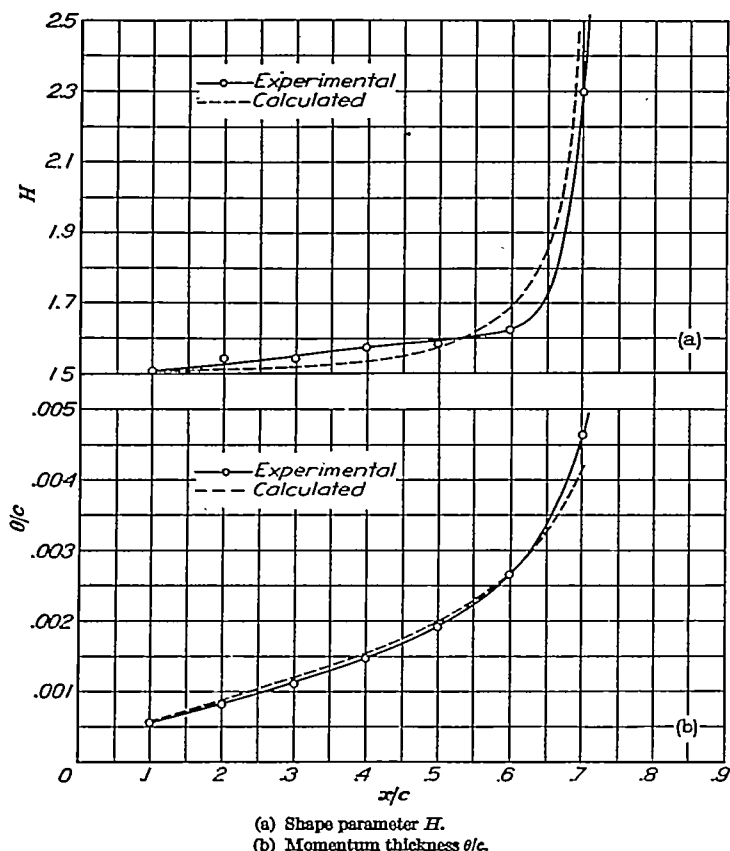
FIGURE 14.—Variation of experimental and calculated values of shape parameter H and momentum thickness θ/c with x/c. NACA 66,2-216, $a=0.6$ airfoil section; $R=2.6 \times 10^6$; $\alpha=10.1°$.

A comparison between the calculated and experimental variations of H and θ along the surface is shown in figures 14 to 24. A computation made by the Gruschwitz method (from reference 8) is included in figure 17. For some of the cases, comparisons of the calculated and experimental boundary-layer profiles at one or two positions are also presented. In general, the calculations are in good agreement with the experimental curves. No systematic differences were found between the calculated and experimental curves of H. Although the agreement between the calculated and experimental curves of θ (figs. 14 to 24) is good in most cases, some consistent differences are apparent as the separation point is approached. In this region, many of the calculated values of θ are less than the experimental values. One explanation of the discrepancy, of course, is that the Squire and Young skin-friction relation is in error in not indicating an increase in skin friction as the boundary-layer velocity profile approaches the shape for separation. This tendency, however, is contrary to the general impression that the skin friction should decrease as the separation point is approached. As the flow approaches separation, the fluctuations in the direction of flow increase. Such fluctuations make a pitot tube read velocities higher than the actual velocities. These fluctuations are a large proportion of the mean flow close to the surface where reversed flow first begins. This behavior of a pitot tube may explain why the turbulent velocity pro-

files, which are close to the separated state, all have the characteristic hump at small values of y/c. The velocity profiles for large values of H are therefore in error in the region close to the surface. The error in profile shape affects θ as well as H. Reading velocities too high for all points where

$\frac{u}{U} < 0.5$ makes the integral for θ, which is $\int_0^{\delta/c} \frac{u}{U}\left(1-\frac{u}{U}\right)d\frac{y}{c}$,

larger than it actually is. It is to be expected, therefore, that values of θ determined by pitot-tube readings should be higher than the true values under conditions of unsteady flow. On the other hand, as separation is approached, the relatively greater velocity fluctuations near the surface may cause the skin friction to be higher than when conditions are far from separation; and the effect of the lower average velocities near the surface, such as occur for higher values of H, may thus be compensated and possibly overbalanced. An attempt was made to correlate the local skin-friction coefficient with H, but no consistent results were obtained. Although there still is considerable doubt concerning the true value of the skin-friction coefficient for conditions approaching separation, it is interesting to note that the Squire and Young skin-friction relation was used through a range of R_θ from 500 to 48,000 and apparently gave good results for most of the region covered by the turbulent boundary layer.

(a) Shape parameter H.
(b) Momentum thickness θ, centimeters.
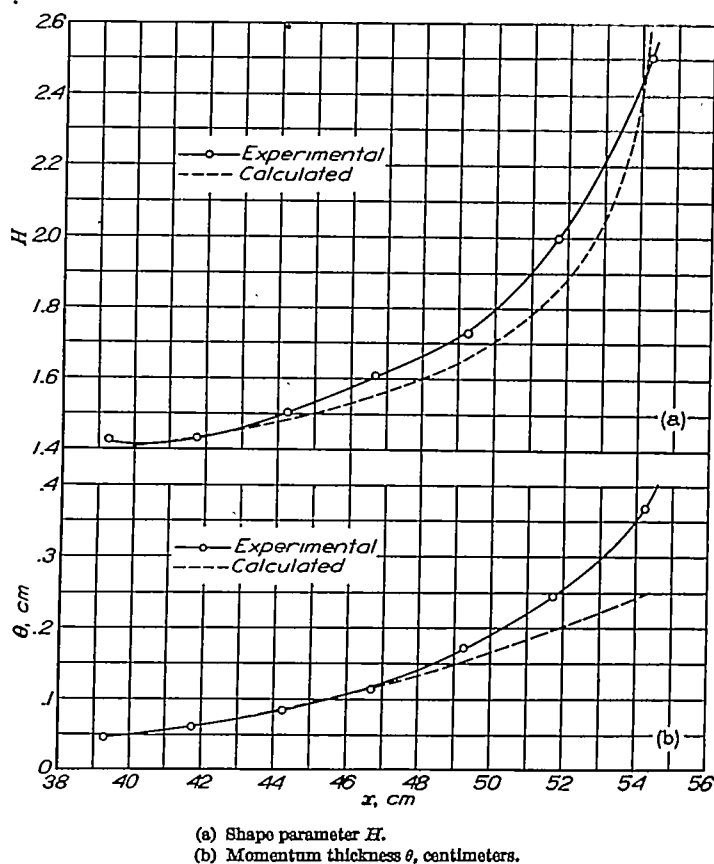
FIGURE 15.—Variation of experimental and calculated values of shape parameter H and momentum thickness θ with x for flow in a channel. (Data from reference 7, run 2.)

(a) $x=46.72$ centimeters.
(b) $x=51.72$ centimeters.
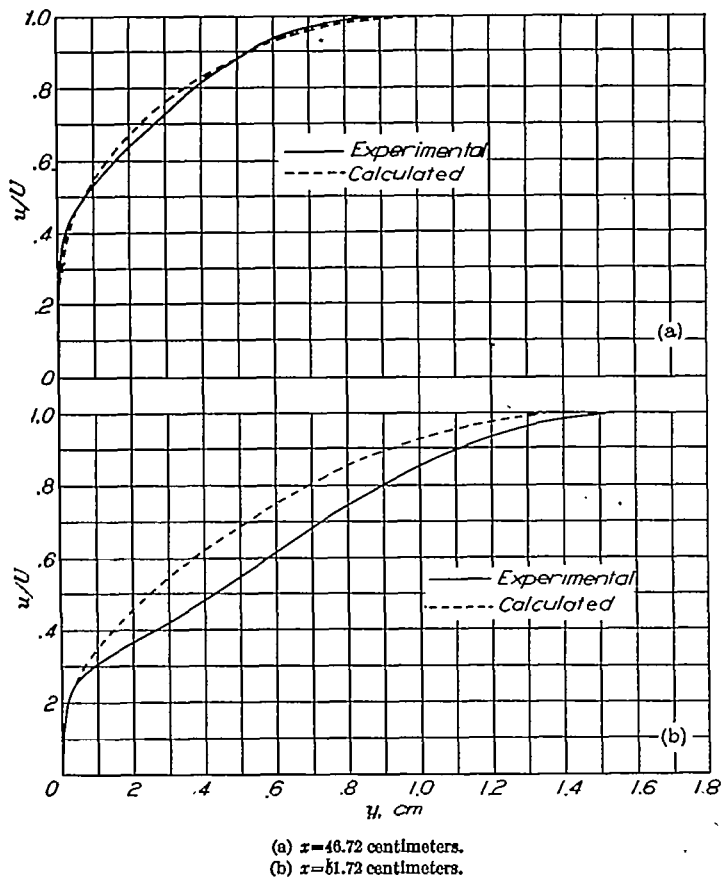
FIGURE 16.—Comparison of experimental and calculated velocity profiles. (Data from reference 7, run 2.)

(a) Shape parameter H.
(b) Momentum thickness θ/D.
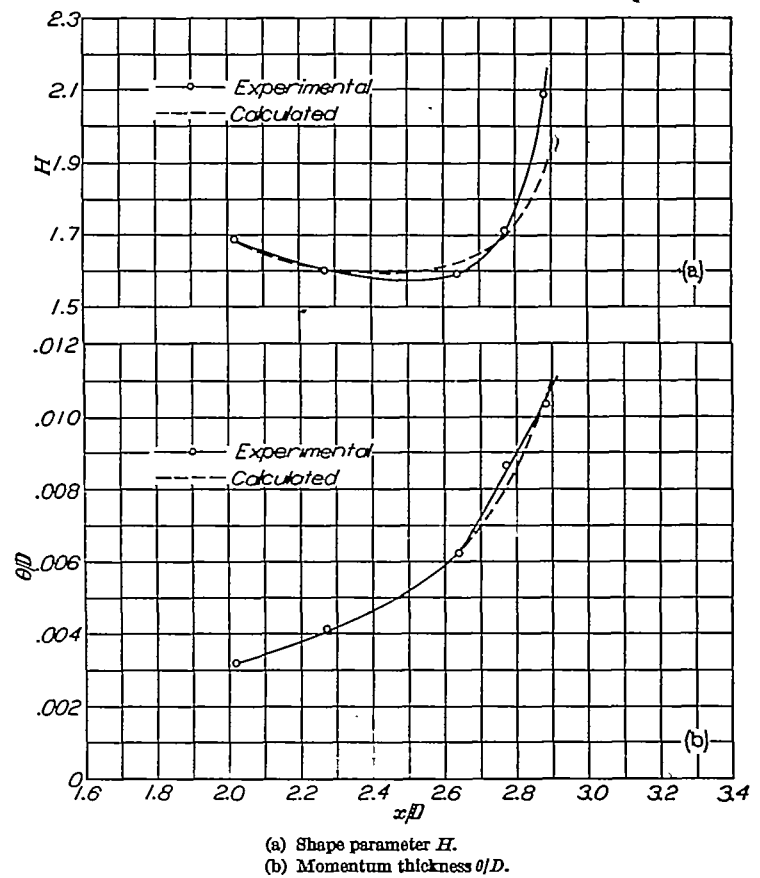
FIGURE 18.—Variation of experimental and calculated values of shape parameter H and momentum thickness θ/D with x/D for elliptic cylinder. $R=118,000$, based on minor axis. (Data from reference 11.)

(a) Shape parameter H.
(b) Momentum thickness θ/c.
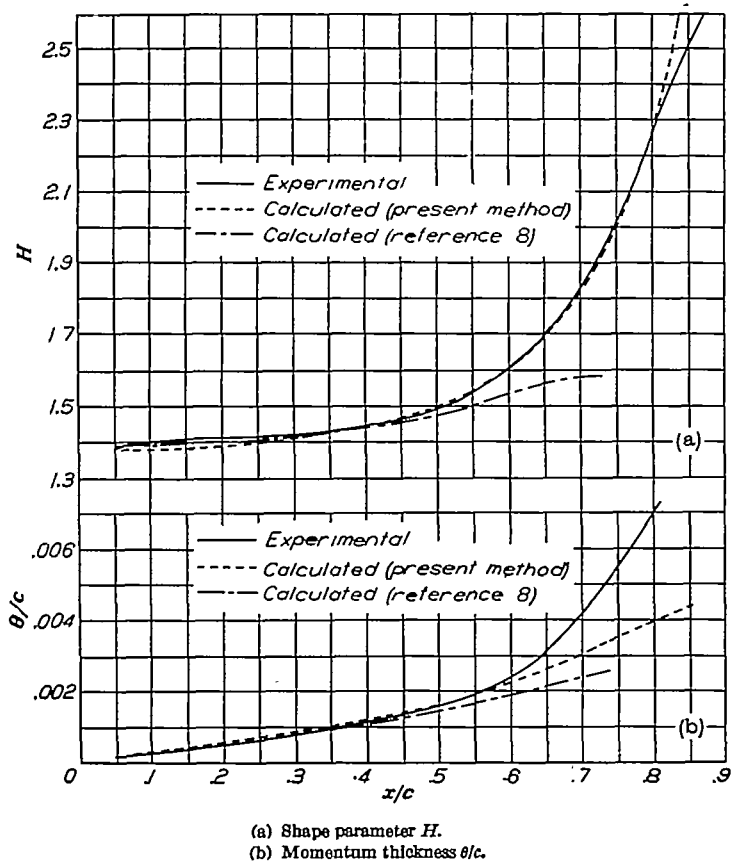
FIGURE 17.—Variation of experimental and calculated values of shape parameter H and momentum thickness θ/c with x/c for symmetrical airfoil. $R=3.8\times10^6$; $\alpha=9°$. (Data from reference 8.)

(a) $\frac{x}{D}=2.77$.

(b) $\frac{x}{D}=2.88$.
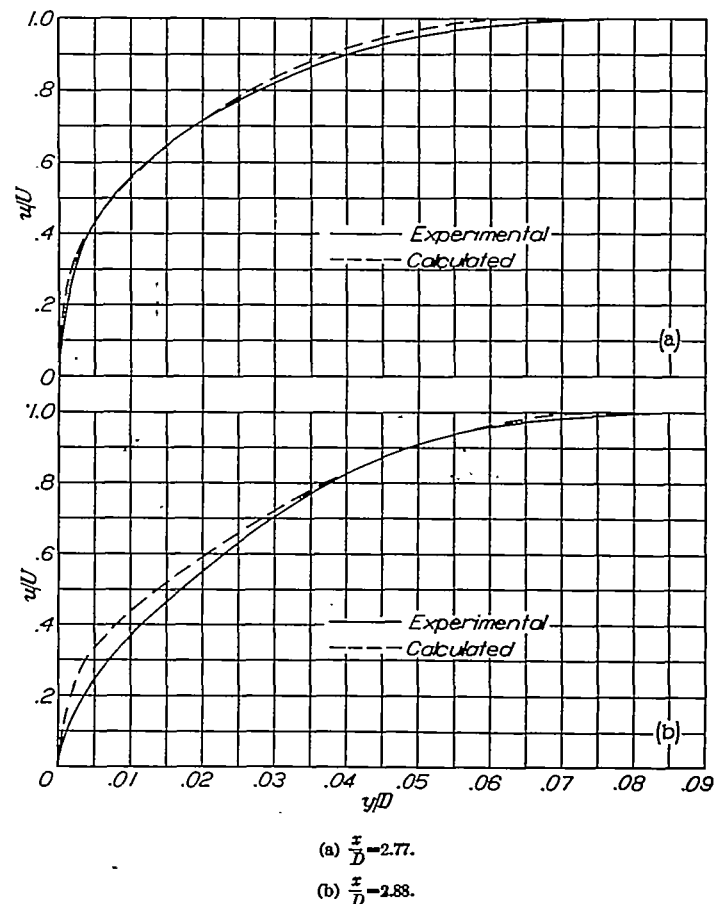
FIGURE 19.—Comparison of experimental and calculated velocity profiles for the elliptic cylinder. $R=118,000$, based on minor axis. (Data from reference 11.)

(a) Shape parameter H.
(b) Momentum thickness θ/c.
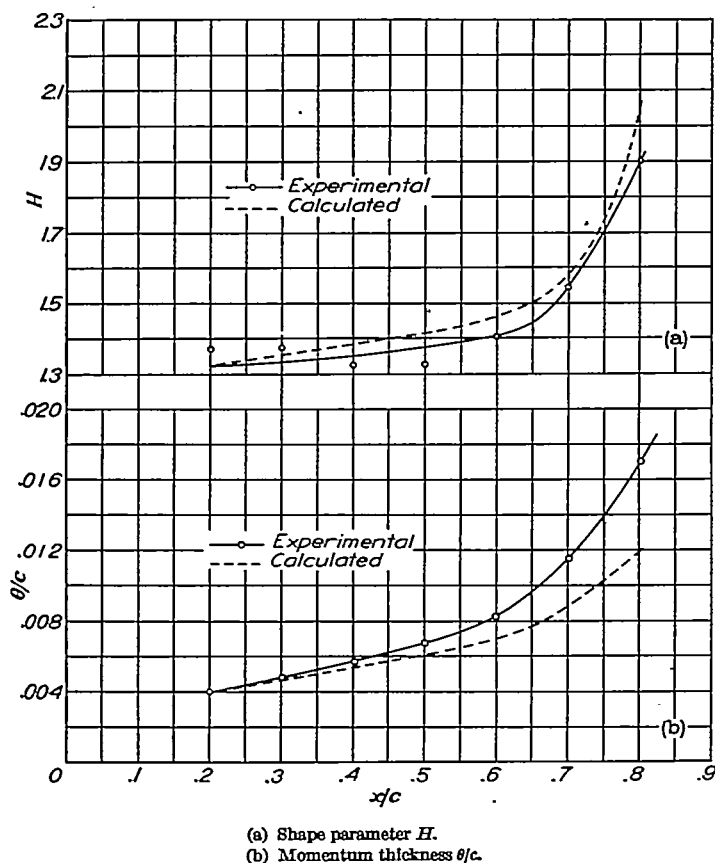
FIGURE 20.—Variation of experimental and calculated values of shape parameter H and momentum thickness θ/c with x/c.   Nose-opening airfoil shape 13; $R=4.18 \times 10^6$; $\alpha=9.1°$.

(a) Shape parameter H.
(b) Momentum thickness θ/c.
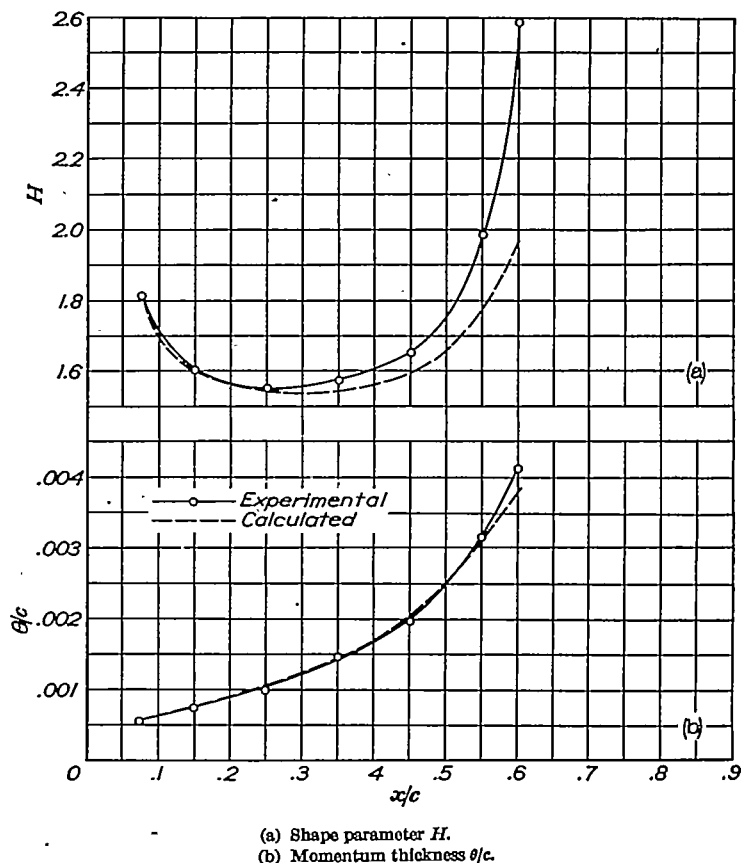
FIGURE 22.—Variation of experimental and calculated values of shape parameter H and momentum thickness θ/c with x/c.   Airfoil section, NACA 65(216)-222 (approx.); $R=0.92 \times 10^6$; $\alpha=8.1°$.
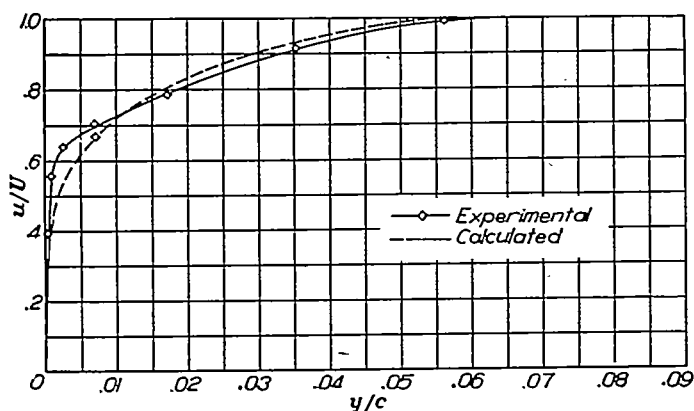
FIGURE 21.—Comparison of experimental and calculated velocity profiles for nose-opening airfoil shape 13. $R=4.18 \times 10^6$; $\alpha=9.1°$; $\frac{x}{c}=.50$.

In making a calculation, the initial condition of the boundary layer must be known.   Computations which have been made do not indicate that the calculation for the H-curve is especially sensitive to the initial value of θ.   When the calculation is to be made for a case in which the boundary layer is in a strong adverse pressure gradient—that is, when $\frac{\theta}{q} \frac{dq}{dx} \frac{2q}{\tau_0}$ is of the same order or greater than $2.035(H-1.286)$— the initial value of H must be accurately determined.   This fact is obvious because the value of H determines how close the flow is to separation.   If the calculation is begun in a region where $\frac{\theta}{q} \frac{dq}{dx} \frac{2q}{\tau_0}$ is very small or positive, the boundary

(a) Shape parameter H.
(b) Momentum thickness θ/c.
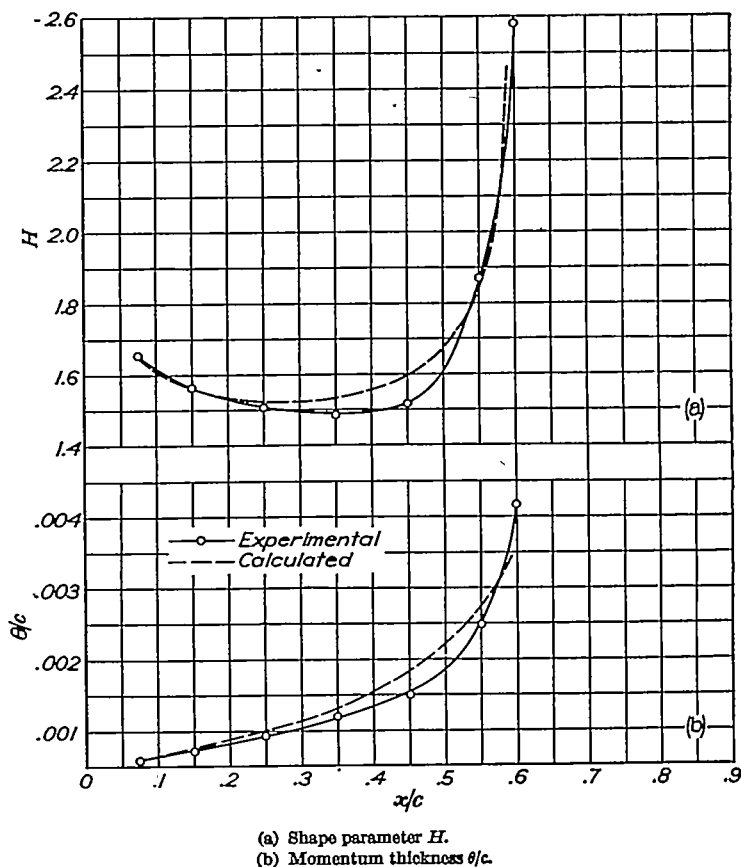
FIGURE 23.—Variation of experimental and calculated values of shape parameter H and momentum thickness θ/c with x/c.   Airfoil section, NACA 65(216)-222 (approx.); $R=2.67 \times 10^6$; $\alpha=8.1°$.

(a) Shape parameter H.
(b) Momentum thickness θ/c.
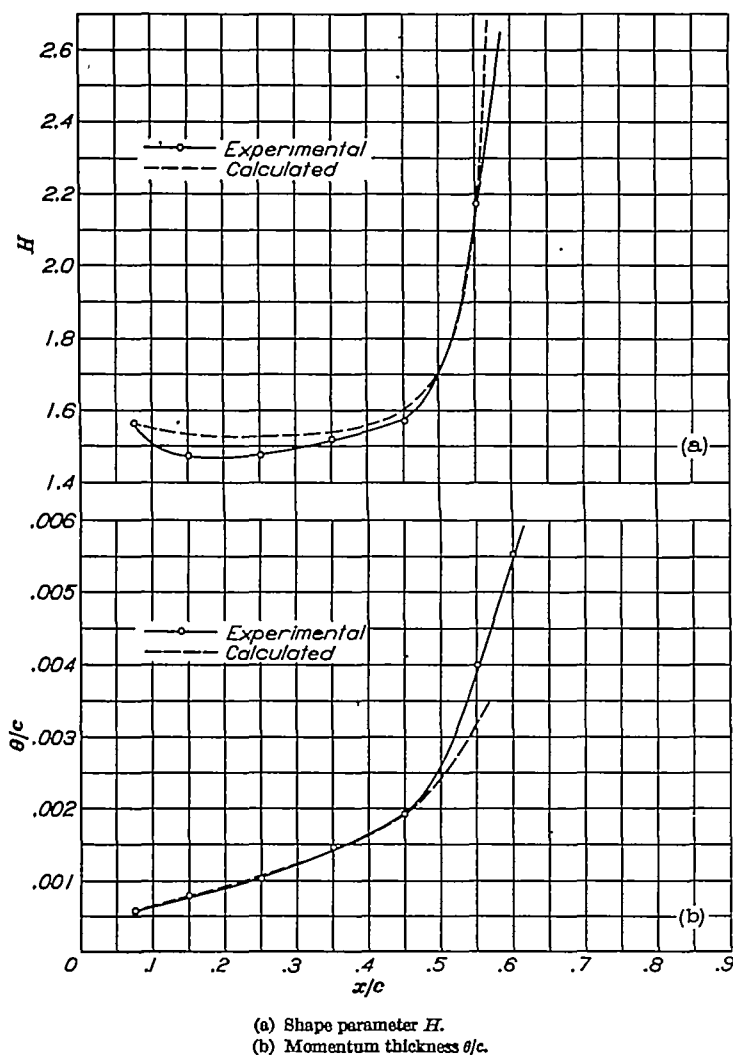
FIGURE 24.—Variation of experimental and calculated values of shape parameter H and momentum thickness θ/c with x/c. Airfoil section, NACA 65(216)-222 (approx.); $R=2.64\times10^6$; $\alpha=10.1°$.

layer is not very sensitive to the initial value of H. For example, if $\frac{dq}{dx}=0$, H will eventually have the value of 1.286 regardless of its initial value.

The boundary-layer thickness is not particularly sensitive to the initial value of H. This effect is easily verified from the form of the momentum equation. The effect of changes in the initial value of θ on the boundary-layer thickness farther downstream depends on the relative magnitude of $\frac{\theta}{q}\frac{dq}{dx}$ and $\frac{\tau_0}{2q}$. If the pressure gradient is large in comparison with the skin friction, a change in the initial value of θ will produce a proportional change in the subsequent values of θ; whereas, if the pressure gradient is small in comparison with the skin friction, a change in the initial value of θ will produce a constant increment equal to the initial change.

The initial value of θ ordinarily may be taken the same as the value for the laminar boundary layer at the transition point. Not enough is known about the mechanism of transition to be able to state in general what the initial values of H should be. If transition occurs in a zero or "favorable" pressure gradient or if the boundary layer is sufficiently thin at the transition point, in accordance with the foregoing

discussion, the position of the turbulent separation point will not be greatly affected by the choice of the initial value of H.

PRESSURE RECOVERY WITHOUT CHANGE IN BOUNDARY-LAYER SHAPE

The equation for $\theta\frac{dH}{dx}$ indicates that, for each value of H, such a value may be assigned to $\frac{\theta}{q}\frac{dq}{dx}$ that $\theta\frac{dH}{dx}=0$. Pressure may be recovered, therefore, without a change in boundary-layer shape if the correct pressure distribution is used. The necessary pressure distribution can be obtained by using the equations for $\frac{dH}{dx}$ and $\frac{d\theta}{dx}$. These equations can be integrated directly if H is assumed to have a constant value. When $\frac{dH}{dx}=0$,

$$\frac{\theta}{q}\frac{dq}{dx}\frac{2q}{\tau_0}=-2.035(H-1.286)=C_1 \qquad (1)$$

where C_1 is a constant. The momentum equation then reduces to the form

$$\frac{d\theta}{dx}=C\frac{\tau_0}{2q} \qquad (2)$$

where

$$C=1+2.035\left(\frac{H+2}{2}\right)(H-1.286)$$

Elimination of $\tau_0/2q$ between equations (1) and (2) gives the relation

$$\frac{1}{C}\frac{d\theta}{dx}=\frac{1}{C_1}\frac{\theta}{q}\frac{dq}{dx}$$

Upon integration,

$$\left(\frac{\theta}{\theta_0}\right)^{\frac{C_1}{C}}=\frac{q}{q_0} \qquad (3)$$

where θ_0 is the initial value of θ and q_0 is the initial value of q. The relations between θ and x and, consequently, between q and x are obtained from integration of equation (2).

For $\tau_0/2q$, the Squire and Young skin-friction relation will be used

$$\frac{\tau_0}{2q}=\frac{1}{[2.557\log_e(4.075\,R_\theta)]^2}$$

$$R_\theta=R_{\theta_0}\left(\frac{\theta}{\theta_0}\right)\left(\frac{q}{q_0}\right)^{1/2}$$

where R_{θ_0} is the initial value of R_θ or

$$R_\theta=R_{\theta_0}\left(\frac{\theta}{\theta_0}\right)\left(\frac{\theta}{\theta_0}\right)^{\frac{C_1}{2C}}$$

Then

$$\frac{\tau_0}{2q}=\frac{1}{\left\{2.557\left[\log_e 4.075R_{\theta_0}+\left(\frac{C_1}{2C}+1\right)\log_e\frac{\theta}{\theta_0}\right]\right\}^2}$$

$$\frac{d\theta}{dx}=\frac{C}{\left\{2.557\left[\log_e 4.075R_{\theta_0}+\left(\frac{C_1}{2C}+1\right)\log_e\frac{\theta}{\theta_0}\right]\right\}^2}$$

The variables are separable. Let

$$E = 2.557 \log_e 4.075 \, R_{\theta_0}$$

$$F = 2.557 \left(\frac{C_1}{2C} + 1 \right)$$

and, when $\frac{\theta}{\theta_0} = 1, \frac{x}{\theta_0} = 0$

The final equation then becomes

$$C \frac{x}{\theta_0} = \left(\frac{\theta}{\theta_0} - 1 \right) (E^2 - 2EF + 2F^2)$$

$$+ 2 \left(\frac{\theta}{\theta_0} \log \frac{\theta}{\theta_0} \right) (EF - F^2) + F^2 \left(\frac{\theta}{\theta_0} \right) \left(\log \frac{\theta}{\theta_0} \right)^2 \quad (4)$$

where

$$C = 1 + 2.035 \left(\frac{H+2}{2} \right) (H - 1.286)$$
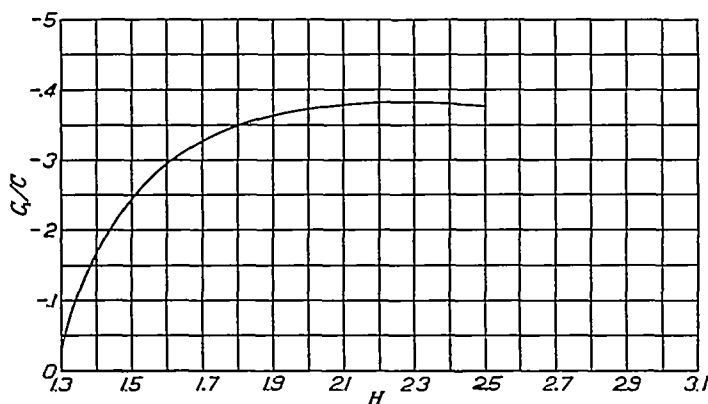
FIGURE 25.—Exponent C_1/C determining rate of pressure recovery for pressure distribution designed to hold a constant H.

By the use of equations (3) and (4), curves of q/q_0 and θ/θ_0 against x/θ_0, which indicate the manner in which pressure can be recovered without a change in boundary-layer shape, may be plotted. Figure 25 is a plot of C_1/C against H, which shows the amount of pressure that can be recovered for a given change in θ as a function of the shape profile to be maintained. The plot indicates that pressure can be recovered at the most rapid rate for a value of H fairly close to the value for separation, that is, about 2.3. Because the flow with such a high value of H is apt to be unsteady, a good compromise between steady flow and minimum increase in θ with decrease in q would seem to be a value of H of 1.7 or 1.8.

CONCLUSIONS

An analysis of a considerable amount of data for turbulent boundary layers collected from the available literature and from tests in the NACA two-dimensional low-turbulence tunnel indicated the following conclusions:

1. The shape of all turbulent-boundary-layer profiles can be expressed as a function of a single parameter.

2. The variables that control the development of the turbulent boundary layer apparently are (1) the ratio of the

nondimensional pressure gradient, expressed in terms of the local dynamic pressure outside the boundary layer and boundary-layer thickness, to the local skin-friction coefficient and (2) the shape of the boundary layer.

3. An empirical equation has been developed in terms of these variables that, when used with the momentum equation and the skin-friction relation, makes it possible to trace the development of the turbulent boundary layer to the separation point.

4. No systematic variation of the skin-friction coefficient with the shape parameter was indicated by the data.

5. Separation occurs for values of the shape parameter greater than 1.8 and less than 2.6.

LANGLEY MEMORIAL AERONAUTICAL LABORATORY,
     NATIONAL ADVISORY COMMITTEE FOR AERONAUTICS,
         LANGLEY FIELD, VA., *April 13, 1943.*

REFERENCES

1. von Doenhoff, Albert E.: A Method of Rapidly Estimating the Position of the Laminar Separation Point. NACA TN No. 671, 1938.
2. Jacobs, E. N., and von Doenhoff, A. E.: Formulas for Use in Boundary-Layer Calculations on Low-Drag Wings. NACA ACR, Aug. 1941.
3. Fluid Motion Panel of the Aeronautical Research Committee and Others: Modern Developments in Fluid Dynamics. Vol. I, S. Goldstein, ed., The Clarendon Press (Oxford), 1938.
4. Nikuradse, Johann: Untersuchungen über die Strömungen des Wassers in konvergenten und divergenten Kanälen. Forsch.-Arb. Geb. Ing.-Wes., VDI-Verlag G. m. b. H. (Berlin), Heft 289, 1929.
5. Dönch, Fritz: Divergente und konvergente turbulente Strömungen mit kleinen Öffnungswinkeln. Forsch.-Arb. Geb. Ing.-Wes., VDI-Verlag G. m. b. H. (Berlin), Heft 282, 1926.
6. Prandtl, L.: The Mechanics of Viscous Fluids. Turbulent Friction Layers in Accelerated and Retarded Flows. Vol. III of Aerodynamic Theory, div. G, sec. 24, W. F. Durand, ed., Julius Springer (Berlin), 1935, pp. 156 and 158.
7. Gruschwitz, E.: Die turbulente Reibungsschicht in ebener Strömung bei Druckabfall und Druckanstieg. Ing.-Archiv, Bd. II, Heft 3, Sept. 1931, pp. 321–346.
8. Peters, H.: On the Separation of Turbulent Boundary Layers. Jour. Aero. Sci., vol. 3, no. 1, Sept. 1935, pp. 7–12.
9. von Doenhoff, Albert E., and Tetervin, Neal: Investigation of the Variation of Lift Coefficient with Reynolds Number at a Moderate Angle of Attack on a Low-Drag Airfoil. NACA CB, Nov. 1942.
10. von Doenhoff, Albert E.: Investigation of the Boundary Layer about a Symmetrical Airfoil in a Wind Tunnel of Low Turbulence. NACA ACR, Aug. 1940.
11. Schubauer, G. B.: Air Flow in the Boundary Layer of an Elliptic Cylinder. NACA Rep. No. 652, 1939.
12. Abbott, Ira H., von Doenhoff, Albert E., and Stivers, Louis S., Jr.: Summary of Airfoil Data. NACA ACR No. L5C05, 1945.
13. von Doenhoff, Albert E., and Horton, Elmer A.: Preliminary Investigation in the NACA Low-Turbulence Tunnel of Low-Drag Airfoil Sections Suitable for Admitting Air at the Leading Edge. NACA ACR, July 1942.
14. Squire, H. B., and Young, A. D.: The Calculation of the Profile Drag of Aerofoils. R. & M. No. 1838, British A. R. C., 1938.

TABLE I.—CALCULATIONS OF θ AND H FOR NACA 65(216)-222 (APPROX.) AIRFOIL SECTION

$[\alpha=10.1^\circ;\ R=2.64\times10^6]$

x/c	θ/c	H	q/q_0	$\frac{c}{q_0}\frac{dq}{dx}$	R_θ	$\frac{\tau_0}{\rho U^2}$	$\frac{H+2}{2}\frac{\theta}{q}\frac{dq}{dx}$	$\frac{d\theta}{dx}$	$\Delta\theta$	$\frac{\theta}{q}\frac{dq}{dx}\frac{2q}{\tau_0}$	$\frac{2.035}{(H-1.286)}$	$\theta\frac{dH}{dx}$	$c\frac{dH}{dx}$	ΔH
0.075	0.574×10⁻³	1.5640	2.550	−2.490	2,382	1.819×10⁻³	−0.998×10⁻³	2.817×10⁻³	2.817×10⁻³	−0.3080	0.566	−0.0003535	−0.616	−0.00616
.085	.6022	1.55794	2.527	−2.385	2,488	1.800	−1.010	2.810	11.24	−.3152	.553	−.0003115	−.517	−.02068
.125	.7146	1.53726	2.448	−2.090	2,903	1.745	−1.082	2.827	2.827	−.3506	.5115	−.0001931	−.2702	−.002702
.135	.7429	1.5346	2.420	−2.065	3,005	1.730	−1.120	2.850	4.275	−.3664	.5059	−.0001660	−.2234	−.003351
.150	.7857	1.52837	2.390	−2.040	3,158	1.708	−1.183	2.891	4.336	−.3926	.4933	−.0001158	−.1474	−.002211
.165	.8291	1.52616	2.360	−2.010	3,312	1.695	−1.245	2.940	10.29	−.4165	.4888	−.0000824	−.09938	−.003478
.200	.9320	1.5227	2.290	−1.990	3,667	1.658	−1.427	3.085	6.17	−.4885	.4817	.0000077	.00826	.000165
.220	.9937	1.52286	2.250	−1.940	3,875	1.639	−1.510	3.149	9.45	−.5229	.4821	.0000465	.0468	.001404
.250	1.0882	1.52426	2.190	−1.800	4,187	1.612	−1.575	3.187	15.935	−.555	.4849	.0000799	.0734	.003670
.300	1.248	1.52793	2.110	−1.600	4,713	1.575	−1.669	3.244	16.220	−.601	.492	.0001254	.1005	.005025
.350	1.410	1.53296	2.022	−1.850	5,213	1.542	−2.316	3.858	3.858	−.850	.503	.000409	.2901	.002901
.36	1.449	1.53586	2.005	−2.000	5,335	1.535	−2.55	4.085	8.170	−.941	.509	.000518	.3575	.007150
.38	1.5307	1.54301	1.960	−2.240	5,572	1.522	−3.098	4.620	9.240	−1.149	.523	.000776	.5070	.01014
.40	1.6231	1.55315	1.910	−2.530	5,832	1.510	−3.820	5.330	10.660	−1.424	.544	.001148	.707	.01414
.42	1.7297	1.56729	1.88	−2.800	6,133	1.495	−4.645	6.140	6.140	−1.742	.572	.001615	1.030	.01030
.43	1.7911	1.57759	1.831	−2.960	6,301	1.488	−5.179	6.667	6.667	−1.946	.593	.001975	1.103	.01103
.44	1.8578	1.58862	1.800	−3.105	6,481	1.477	−5.75	7.227	7.227	−2.170	.616	.002393	1.2881	.012881
.45	1.9369	1.60150	1.770	−3.290	6,700	1.470	−6.483	7.953	7.953	−2.449	.642	.002945	1.520	.01520
.46	2.0164	1.61670	1.731	−3.455	6,898	1.455	−7.279	8.734	8.734	−2.766	.673	.003684	1.827	.01827
.47	2.104	1.63497	1.700	−3.620	7,132	1.448	−8.142	9.590	4.795	−3.094	.710	.004577	2.175	.01088
.475	2.1520	1.64585	1.682	−3.700	7,257	1.442	−8.630	10.075	5.038	−3.276	.732	.00511	2.375	.01188
.48	2.2024	1.65773	1.663	−3.800	7,384	1.441	−9.199	10.640	5.320	−3.493	.755	.00586	2.661	.01330
.485	2.2556	1.67103	1.645	−3.880	7,522	1.435	−9.765	11.200	5.600	−3.707	.783	.00661	2.930	.01465
.49	2.3116	1.68568	1.625	−3.970	7,661	1.430	−10.41	11.840	5.920	−3.949	.813	.007589	3.283	.01642
.495	2.3708	1.70210	1.608	−4.080	7,816	1.422	−11.14	12.56	6.280	−4.233	.847	.00837	3.741	.01870
.50	2.4336	1.72080	1.586	−4.170	7,968	1.420	−11.91	13.33	6.665	−4.507	.885	.01036	4.257	.02128
.505	2.5002	1.74208	1.566	−4.222	8,135	1.413	−12.61	14.02	7.010	−4.770	.928	.01210	4.840	.02420
.51	2.570	1.76628	1.545	−4.262	8,306	1.406	−13.35	14.76	7.380	−5.043	.977	.01431	5.568	.02784
.515	2.6438	1.79412	1.525	−4.282	8,489	1.401	−14.08	15.48	7.740	−5.296	1.034	.01709	6.464	.03232
.52	2.7212	1.82644	1.500	−4.292	8,665	1.395	−14.90	16.30	8.150	−5.584	1.100	.02085	7.662	.03831
.525	2.8027	1.86495	1.475	−4.290	8,850	1.391	−15.75	17.14	8.570	−5.859	1.178	.02621	9.352	.04676
.530	2.8894	1.91171	1.450	−4.265	9,043	1.384	−16.62	18.00	9.002	−6.142	1.273	.03408	11.7989	.05899
.535	2.9784	1.97070	1.431	−4.080	9,284	1.375	−16.88	18.74	9.370	−6.175	1.393	.04399	14.770	.07385
.54	3.0721	2.04455	1.407	−3.380	9,474	1.373	−14.92	16.29	8.145	−5.375	1.544	.05019	16.337	.08168
.545	3.1536	2.12623	1.390	−3.000	9,667	1.368	−14.05	15.42	7.710	−4.978	1.710	.06242	19.793	.09896
.55	3.2307	2.22519	1.374	−2.650	9,846	1.362	−13.16	14.52	7.260	−4.575	1.911	.07992	24.738	.12369
.555	3.3033	2.34888	1.362	−2.340	10,023	1.357	−12.34	13.70	6.850	−4.182	2.163	.10631	32.334	.16167
.56	3.3718	2.51055	1.354	−2.080	10,201	1.352	−11.68	13.03	6.515	−3.831	2.492	.15131	44.875	.22438
.565	3.4370	2.73493												